2013

Graph rigidity-based formation control of planar multi-agent systems

Xiaoyu Cai
Louisiana State University and Agricultural and Mechanical College, xcai2@lsu.edu

GRAPH RIGIDITY-BASED FORMATION CONTROL OF PLANAR MULTI-AGENT SYSTEMS

A Dissertation

Submitted to the Graduate Faculty of the
Louisiana State University and
Agricultural and Mechanical College
in partial fulfillment of the
requirements for the degree of
Doctor of Philosophy

in

The Department of Mechanical and Industrial Engineering

by
Xiaoyu Cai
B.S., Mechanical Engineering, Shanghai Jiao Tong University, China, 2009
August 2013

Acknowledgements

I would like to express sincere appreciation to my advisor, Dr. Marcio de Queiroz. Without his guidance and persistent help, this dissertation would not have been possible. I would also like to thank my committee members, Dr. Yitshak Ram, Dr. Kemin Zhou, Dr. John Pojman, and Dr. Michael Malisoff, for their time and valuable suggestions. Finally, I would like to thank the National Science Foundation, through grant ECCS-1102348, and the LSU Department of Mechanical and Industrial Engineering for their financial support.

Table of Contents

List of Figures

Abstract

A multi-agent system is a network of interacting "agents" that collectively perform a complex task. This dissertation is concerned with the decentralized formation control of multi-agent systems moving in the plane. The formation problem is defined as designing control inputs for the agents so that they form and maintain a pre-defined, planar geometric shape. The focus is on three related problems with increasing level of complexity: *formation acquisition*, *formation maneuvering*, and *target interception*. Three different "dynamic" models, also with increasing level of complexity, are considered for the motion of the agents: the single-integrator model, the double-integrator model, and the full mechanical dynamic model. Rigid graph theory and Lyapunov theory are the primary tools utilized in this work for solving the aforementioned formation problems for the three models. The backstepping control technique also plays a key role in the cases of the double-integrator and full dynamic models.

Starting with the single-integrator model, a *basic* formation acquisition controller is proposed that is only a function of the relative position of agents in an infinitesimally and minimally rigid graph. A Lyapunov analysis shows that the origin of the inter-agent distance error system is exponentially stable. It is then shown how an extra term can be added to the controller to enable formation maneuvering or target interception. The three controllers for the single-integrator model are used as a stepping stone and extended to the double-integrator model with the aid of backstepping. Finally, an actuator-level, formation acquisition control law is developed for multiple robotic vehicles that accounts for the vehicle dynamics. Specifically, a class of underactuated vehicles modeled by Euler-Lagrange-like equations is considered. The backstepping technique is again employed while exploiting the structural properties of the system dynamics. Computer simulations are provided throughout the dissertation to show the proposed control laws in action.

Chapter 1 Introduction

1.1 Motivation

A multi-agent system refers to a network of interacting "agents" that collectively perform a complex task beyond their individual capabilities. The concept is inspired by the collective behavior of biological systems in nature, e.g., flock of birds, school of fish, and colony of bees. Interestingly, the behavior of such biological swarms is distributed and decentralized as each biological agent operates using its own local sensing and control mechanisms devoid of global knowledge or planning [20]. Many engineering multi-agent systems have been developed to mimic this coordinated behavior. One example is a group of autonomous (ground, underwater, water surface, or air) vehicles performing surveillance, reconnaissance, mapping, or search of an area. Another example is a military mission where a group of unmanned air vehicles surround and intercept an intruding aircraft. Recent advances in sensor technology, computer processing, communication systems, and power storage now make it feasible to deploy such swarms of coordinated, cooperating vehicles in various environments.

Multi-agent systems offer many advantages over a large, single agent such as more efficient and complex task execution, robustness when one or more agents fail, scalability, versatility, adaptability, and lower cost. However, they introduce a host of unique challenges: coordination and cooperation among agents, distribution of information and subtasks, communication protocols, design of control laws, and collision avoidance.

Among the many coordination and cooperation problems for multi-agent systems (e.g., aggregation, social foraging, flocking, and swarm formation), we are interested here in the class of *formation* problems. Specifically, our focus is on three related problems with increasing level of complexity: *formation acquisition*, which is defined as designing control inputs for the agents so that they form a pre-defined, fixed geometric shape in space; *formation maneuvering*, where agents are required to simultaneously acquire a formation and move cohesively following a pre-defined (time-varying) trajectory; and *target interception*, where agents intercept and surround a moving target with a pre-defined formation. Note that formation acquisition is a pre-condition for formation maneuvering and target interception.

Accurate knowledge and control of the agents' relative position in the formation are critical for solving the aforementioned problems. This, in turn, is heavily dependent on the model of the agents' motion used to design the formation controller. A common approach is to design a "high-level" control law by assuming that the agent motion is governed by the single-integrator (kinematic) model with velocity-level control inputs. Another common, but lower level, approach is to use the double-integrator (point mass) model for each robot with acceleration-level control inputs. Neither of these simplified approaches can be directly implemented on an actual multi-agent system since they do not provide actuator-level (i.e., force/torque) inputs. At best, they can be embedded (as inner control loops) in a non-model-based, actuator-level control system that neglects the agent dynamics.

Formation control problems are relatively straightforward to solve when the agents' absolute coordinates (i.e., w.r.t. an Earth-fixed coordinate frame) are available via a central planner. From this information, the relative position of agents can be readily calculated and transmitted to each one. However, as pointed out in [26], a global positioning system (GPS), which is typically used in such cases, has limited accuracy when there is no line of sight between the GPS receiver and satellite (e.g., urban areas, dense vegetation, and dense clouds). Therefore, we consider here the *decentralized* formation problem where each agent has only locally-sensed information about the other agents and target obtained from a suite of onboard sensors, such as an inertial-type navigation system, laser range finder, camera, and/or compass.

Graph theory, specifically the concepts of graph Laplacian and graph rigidity, is a natural tool for describing the multi-agent formation shape and the inter-agent sensing and communication network topology in the decentralized case. The research in this dissertation is based on rigid graph theory since it naturally ensures that the inter-agent distance constraints of the desired formation are enforced through the graph rigidity. The concept of graph rigidity is analogous to the rigidity of civil structures. In our case, the "vertices" of the "structure" are the agents and the "bars" connecting the vertices are the inter-agents distance constraints imposed by the desired formation. In this framework, it is convenient to treat each agent as a point and model their motion with the single-integrator equation. As a result, most graph rigidity-based formation control results

utilize the single-integrator model (see literature review below). In this dissertation, we will go beyond this approach and introduce results are that based on the double-integrator model and, subsequently, on the full dynamic model.

1.2 Literature Review

Some of the earliest work to apply graph theory to multi-agent formation can be found in [3, 10, 16, 18, 35, 45]. An overview of rigid graph theory and its application to sensing, communication, and control architectures for formations of autonomous vehicles was presented in [1]. A comprehensive coverage of graph Laplacian-based formation control can be found in [41].

Results on formation acquisition based on controlling inter-agent distances using the single-integrator model and rigid graph theory can be found in [5, 14, 15, 26, 33, 44]. Other single-integrator results not based on rigid graphs were presented in [12, 43]. Specifically, [12] proposes an aggregation algorithm that is the sum of a repulsive potential field for collision avoidance and an attractive potential field for convergence to the desired configuration. In [43], control techniques for redundant robot manipulators were applied to the formation problem.

In [34], a rigidity-based formation maneuvering controller was proposed using the single-integrator model for cycle-free persistent formations under the condition that the trajectory velocity is sufficiently low. A relative position-based formation maneuvering protocol was introduced in [47] for the single-integrator model that ensures formation acquisition in finite time. A collaborative target tracking controller based on flocking and Kalman-type filtering algorithms was given in [37] using the double-integrator agent model. In [20], distance-based formation maneuvering and target interception schemes were designed using the single-integrator model by adding terms to a gradient-of-potential-function law. In one of the target interception schemes in [20], the absolute velocity of the target is uncertain but with known bound and a variable structure-type control is designed to compensate for the unknown velocity. The double-integrator model was used in [36] where maneuvering of the flocking agents was achieved by adding a dynamic virtual leader-dependent term to the control scheme. Recently, [30] used an iterative learning controller to ensure finite-time formation maneuvering with bounded tracking error.

Some work has explicitly accounted for the agent dynamics during the design of formation con-

trollers. For example, [6, 7, 25, 28, 39] use fully-actuated Euler-Lagrange equations to model each agent in the swarm. This model accounts for fully-actuated robot manipulators, spacecraft, and mobile robots. Specifically, [7] designed a synchronization tracking controller for the cooperative multi-agent system. A finite-time consensus tracking controller for multi-agent systems was proposed in [25]. In [39], a robust adaptive formation controller was designed under the assumption of the presence of parameter uncertainties in the system model. Under the assumption of functional uncertainties, [6] designed a neural network controller that ensures the multi-agent system synchronizes to the motion of a dynamic target. In [28], a passive decomposition approach was used to decouple the solution of formation acquisition and formation maneuvering problems. The model of a differentially-driven, wheeled mobile robot with nonholonomic constraints was used in [29] to design a formation control scheme that maintains the prescribed formation while avoiding obstacle and inter-vehicle collisions. In [38], an adaptive neural network controller was proposed for formations of marine vessels with uncertain dynamics using the dynamic surface control technique.

1.3 Dissertation Organization

This dissertation introduces a class of graph rigidity-based formation controllers for multi-agent systems whose motion is restricted to the plane. Our control laws stabilize the inter-agent distance dynamics to desired distances using various system models, viz., single integrator, double integrator, and full mechanical dynamics. In addition to concepts of rigid graph theory, our control designs exploit Lyapunov theory [24] and the backstepping control technique [27].

We begin by introducing in Chapter 2 the basic concepts of rigid graph theory and some related preliminaries results which are used in subsequent chapters. Here, we prove a key claim made in [33] regarding the infinitesimal rigidity of "close" frameworks (see Lemma 2.2). This preliminary result plays an important role in formalizing the subsequent Lyapunov stability analyses.

We naturally begin the formation control formulation with the simple single-integrator model in Chapter 4. Here, we first design a formation acquisition controller for n agents modeled by an undirected graph. The desired inter-agent distances are imposed such that the resulting graph is infinitesimally and minimally rigid. Our control law, which is dependent on the rigidity matrix

of the graph, ensures that the desired formation is exponentially stable. The proposed control is distributed in the sense that the control input of each agent is only a function of the relative position of neighboring agents in the graph. The formation acquisition controller is a basic control term since it will appear in all other control algorithms developed in this dissertation. Building upon this result, we show how the formation acquisition control can augmented with a term to enable the agents to perform formation maneuvering or target interception simultaneously with formation acquisition. In the formation maneuvering problem, the swarm (group) velocity is known to all agents. We then extend the idea behind the control design for formation maneuvering to the target interception problem. In this case, we use the leader-follower concept by assigning the leader role to one agent in the formation, who is responsible for tracking the moving target. We assume the target's relative position to the leader is known and can be broadcast to the followers; however, the target's velocity is *unknown* to all agents. To deal with this uncertainty, the target interception component of the control law will contain a continuous dynamic robust mechanism, inspired by the work in [46], to "estimate" the target velocity. The graph that models the desired formation in this case is constructed with the additional property that the leader is in the convex hull of the followers. As a result, the proposed control ensures the followers eventually enclose the target. Our stability analysis for both problems provides exponential formation acquisition and asymptotic formation maneuvering or target tracking.

The contributions of Chapter 4 are the following: 1) To the best of our knowledge, we are the first to extend the rigidity matrix-based approach to the formation maneuvering and target interception problems ([5, 14, 15, 26, 33, 44] only address the formation acquisition problem); 2) We do not require the trajectory velocity in the formation maneuvering problem to be sufficiently low as in [34]; 3) We do not need to measure the relative position of all agents as in [20]. Rather, we only require measurement of this variable for agents connected in the infinitesimally and minimally rigid graph; 4) We do not require absolute position measurements as in [30, 47]; and 6) Our target interception control law is continuous, unlike the one in [20].

In Chapter 5, we use the double-integrator model for the agents' motion by exploiting the back-stepping control technique. Backstepping is a natural tool for solving this problem since it allows

us to treat the velocity-level inputs designed in Chapter 4 as *fictitious* control inputs, which are to be tracked by the new, acceleration-level inputs. The formation acquisition control law in this chapter also ensures that the desired formation is exponentially stable. It is decentralized in the sense that the control input of each agent is only dependent on the relative position and relative velocity of neighboring agents in the graph and the agents' own velocity. The formation maneuvering control is dependent on the desired swarm acceleration in addition to the velocity. In the target interception problem, we assume the target's relative position to the leader and velocity are known and can be broadcast to the followers; however, the target's *acceleration* is unknown to all agents. To deal with this uncertainty, the target interception component of the control law will contain a variable structure-type term to compensate for the unknown target acceleration. The stability results of the previous chapter are preserved. The contribution of this chapter is that, although there are some multi-agent results in the literature based on the double-integrator model (e.g., [20, 21, 36, 32]), we are the first to solve the formation acquisition, formation maneuvering, and target interception problems within the framework of rigid graph theory.

In Chapter 6, we fully account for the mechanical dynamics of each agent during the control design process. The control here is limited to the formation acquisition problem. We consider a class of underactuated robotic vehicles moving on the plane, such as wheeled mobile robots, marine (surface) vessels, underwater vehicles with constant depth, and aircraft with constant altitude. The equations of motion are first transformed into an Euler-Lagrange-like dynamic model so we can exploit its structural properties in the control design and stability analysis. The formation acquisition control formulation builds upon the results from the previous chapters. Specifically, the backstepping technique is reapplied to embed the velocity-level inputs from Chapter 4 in the actuator-level control law in a rigorous manner. A Lyapunov analysis shows that, under the proposed control, the inter-robot distance error dynamics is exponentially stable at the origin. To the best of our knowledge, we are the first to combine the graph rigidity-based formation acquisition control method with dynamic compensation.

Simulation results are provided in Chapters 4 to 6 to demonstrate the proposed controllers. Conclusions and suggestions for future work are presented in Chapter 7.

Chapter 2 Rigid Graph Theory: Preliminary Results

The control algorithms in this dissertation rely on some basic concepts of rigid graph theory in $\mathbb{R}^2$, which are outlined below. An in-depth coverage of these concepts can be found in, for example, [1, 2, 8, 11, 22, 23, 42].

An undirected graph G is a pair (V, E) where $V = \{1, 2, \ldots, n\}$ is the set of vertices and $E \subset V \times V$ is the set of undirected edges such that if vertex pair $(i, j) \in E$ then so is (j, i). The number of edges l is given by $l \in \{1, \ldots, n(n-1)/2\}$. Let the set of neighbors of vertex i be denoted by

$$\mathcal{N}_i(E) = \{j \in V \mid (i, j) \in E\}. \tag{2.1}$$

If $p_i \in \mathbb{R}^2$ is the coordinate of vertex i, then a framework F is a pair (G, p) where $p = (p_1, \ldots, p_n) \in \mathbb{R}^{2n}$. That is, a framework is simply a realization of the graph at given points in the plane.

Based on an arbitrary ordering of the edges in E, the edge function $\phi_E : \mathbb{R}^{2n} \to \mathbb{R}^l$ is given by

$$\phi_E(p) = \left(\ldots, \|p_i - p_j\|_2^2, \ldots\right), \quad (i, j) \in E. \tag{2.2}$$

The kth component of (2.2), $\|p_i - p_j\|_2^2$, corresponds to the kth edge in E connecting vertices i and j. It is not difficult to show that (2.2) is invariant under isometric motions (rotation, translation, and reflection) of $F = (G, p)$ [1, 26, 42]. The rigidity matrix $R : \mathbb{R}^{2n} \to \mathbb{R}^{l \times 2n}$ of F is defined as

$$R(p) = \frac{1}{2}\frac{\partial \phi_E(p)}{\partial p}, \tag{2.3}$$

which has the property that [2]

$$\text{rank}\,[R(p)] \leq 2n - 3. \tag{2.4}$$

An isometry of $\mathbb{R}^2$ is a bijective map $T : \mathbb{R}^2 \to \mathbb{R}^2$ such that [22]

$$\|x - y\|_2 = \|T(x) - T(y)\|_2, \quad \forall x, y \in \mathbb{R}^2 \tag{2.5}$$

where $\|\cdot\|_2$ denotes the Euclidean norm. Note that T accounts for rotation, translation, and reflection of the vector $x - y$. We denote the set of all isometries of $\mathbb{R}^2$ by Iso($\mathbb{R}^2$).

Two frameworks (G, p) and $(G, \hat{p})$ are equivalent if $\phi_E(p) = \phi_E(\hat{p})$, and are congruent if $\|p_i - p_j\|_2 = \|\hat{p}_i - \hat{p}_j\|_2$ for all $i, j \in V$ [23]. A framework (G, p) is globally rigid if and only if all frameworks equivalent to (G, p) differ only by isometric motions. Note that a non-globally rigid framework can be made globally rigid by adding edges to its graph. We say a framework $F = (G, p)$, where the affine span of p is all of $\mathbb{R}^2$, is infinitesimally rigid if and only if

rank$[R(p)] = 2n - 3$ [8]. A framework $F = (G, p)$ is minimally rigid if $l = 2n - 3$. If two infinitesimally rigid frameworks (G, p) and $(G, \hat{p})$ are equivalent but not congruent, then they are said to be *flip ambiguous* [1] (see Figure 2.1(b) for an example). Note that a globally rigid framework does not have flip ambiguities since "fold-overs" such as in 2.1(b) are not isometric motions.

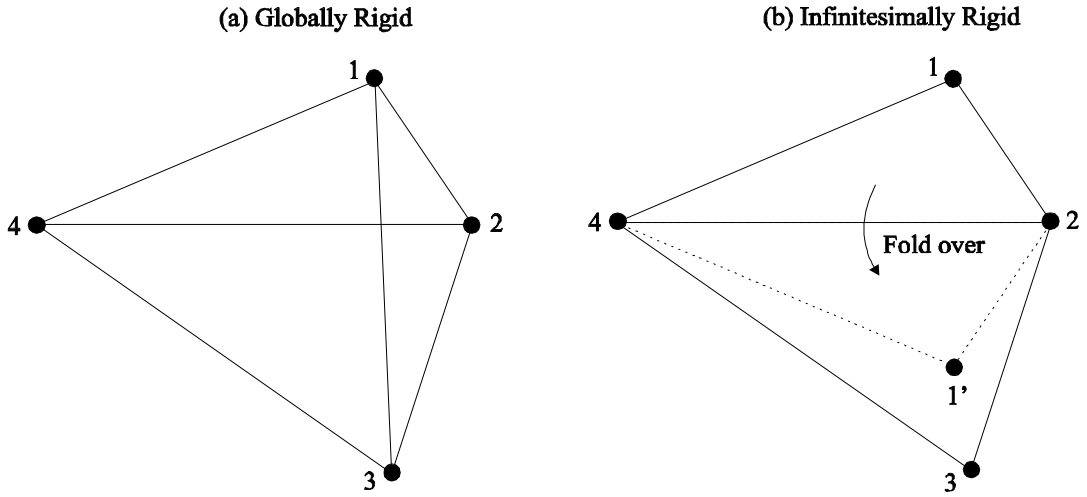

Figure 2.1: (a) The globally rigid framework F_g. (b) An infinitesimally rigid framework F_I uniquely obtained by removing edge $(1, 3)$, and a possible equivalent realization with flipped edges $(1', 2)$ and $(1', 4)$.

The lemmas and corollary below will be vital for establishing our main result in a rigorous manner. Specifically, they will allow us to formalize the stability set of the closed-loop system in relation to the infinitesimal rigidity and potential flip ambiguities of the framework modeling the formation. The following notation is used throughout these preliminaries results. Given a point ζ and a set $\mathcal{M}$, [24]

$$\text{dist}\,(\zeta, \mathcal{M}) = \inf_{x \in \mathcal{M}} \|\zeta - x\|_2 . \tag{2.6}$$

Consider a globally rigid framework $F_g = (G_g, p)$ where $G_g = (V, E_g)$, $\dim(V) = n$, and $\dim(E_g) = l_g$. Up to isometric motions, the realization for the edge function of F_g is *unique* and given by $\phi_{E_g}^{-1}\left(\phi_{E_g}(p)\right)$.[1] We can arbitrarily remove edges from G_g to obtain an infinitesimally rigid framework $F_I = (G_I, p)$ where $G_I = (V, E_I)$, $E_I \subseteq E_g$, and $\dim(E_I) = l_I \leq l_g$. Note that F_I is uniquely defined by this construction since it eliminates flip realizations of its edge function $\phi_{E_I}(p)$. An example is shown in Figure 2.1.

[1] The function $\phi_{E_g}^{-1}\left(\phi_{E_g}(p)\right)$ has infinite solutions due to isometric motions. However, since F_g is globally rigid, all resulting frameworks are congruent. Therefore, we say that the realization of $\phi_{E_g}(p)$ is unique.

Lemma 2.1 Consider the set

$$\mathcal{H}(p) = \left\{\hat{p} \in \mathbb{R}^{2n} \mid \hat{p}_i = T\left(p_i\right),\ i = 1, , ..., n,\ \forall T \in \text{Iso}\left(\mathbb{R}^2\right)\right\} \tag{2.7}$$

where T was defined in (2.5). Given a constant $\varepsilon > 0$, if $\text{dist}(\bar{p}, \mathcal{H}(p)) \leq \varepsilon$, then there exists constants $\delta_{ik}\left(\varepsilon\right) > 0$, $i = 1, ..., n$, $k = 1, 2$ and an isometry $\bar{T} \in \text{Iso}(\mathbb{R}^2)$ such that

$$\left[\bar{p}_i\right]_k = \left[\bar{T}\left(p_i\right)\right]_k + \delta_{ik} \tag{2.8}$$

where $\left[\cdot\right]_k$ denotes the kth element of the vector.

Proof. From (2.6) and (2.7), we have

$$\text{dist}\left(\bar{p}, \mathcal{H}(p)\right) = \inf_{T(p_i) \in \mathcal{H}(p)} \sqrt{\sum_{i=1}^{n} \left\|\bar{p}_i - T\left(p_i\right)\right\|_2^2}. \tag{2.9}$$

Take $\bar{T} \in \text{Iso}(\mathbb{R}^2)$ such that

$$\inf_{T(p_i) \in \mathcal{H}(p)} \sqrt{\sum_{i=1}^{n} \left\|\bar{p}_i - T\left(p_i\right)\right\|_2^2} = \sqrt{\sum_{i=1}^{n} \left\|\bar{p}_i - \bar{T}\left(p_i\right)\right\|_2^2}. \tag{2.10}$$

Since $\text{dist}(\bar{p}, \mathcal{H}(p)) \leq \varepsilon$, we have

$$\sum_{i=1}^{n} \left\|\bar{p}_i - \bar{T}\left(p_i\right)\right\|_2^2 \leq \varepsilon^2 \tag{2.11}$$

Let $\varepsilon^2 = \sum_{i=1}^{n} \alpha_i$ where α_i is a positive constant, then

$$\sum_{i=1}^{n} \left\|\bar{p}_i - \bar{T}\left(p_i\right)\right\|^2 - \alpha_i \leq 0. \tag{2.12}$$

A sufficient condition for (2.12) is given by

$$\left\|\bar{p}_i - \bar{T}\left(p_i\right)\right\|^2 - \alpha_i \leq 0, \quad i = 1, ..., n. \tag{2.13}$$

Thus, we can write

$$\left(\bar{p}_i - \bar{T}\left(p_i\right)\right)^T \left(\bar{p}_i - \bar{T}\left(p_i\right)\right) - \alpha_i = -\sigma_i, \quad 0 < \sigma_i \leq \alpha_i, \quad i = 1, ..., n. \tag{2.14}$$

Let $\alpha_i - \sigma_i = \delta_i^T \delta_i$ where $\delta_i = \left(\delta_{i1}, \delta_{i2}\right) = \left(\sqrt{\left(\alpha_i - \sigma_i\right)/2}, \sqrt{\left(\alpha_i - \sigma_i\right)/2}\right)$. Then, it follows from (2.14) that

$$\bar{p}_i - \bar{T}\left(p_i\right) = \delta_i, \quad i = 1, ..., n \tag{2.15}$$

or

$$\left[\bar{p}_i\right]_k = \left[\bar{T}\left(p_i\right)\right]_k + \delta_{ik}, \quad i = 1, ..., n,\ k = 1, 2. \tag{2.16}$$

■

Lemma 2.2 If $F = (G, p)$ is infinitesimally rigid, then so is $\bar{F} = (G, \bar{p})$ if the point $\bar{p}$ is sufficiently close to $\mathcal{H}(p)$ of (2.7).

Proof. Given that $\|\hat{p}_i - \hat{p}_j\|_2 = \|T(p_i) - T(p_j)\|_2$, $(i,j) \in E$, then $\phi_E(\hat{p}) = \phi_E(p)$ and rank$[R(\hat{p})]$ = rank$[R(p)] = 2n-3$ since $F = (G, p)$ is infinitesimally rigid. Therefore, $\hat{F} = (G, \hat{p})$ is also infinitesimally rigid.

Since rank$[R(\hat{p})] = 2n - 3$, there exists a $(2n-3) \times (2n-3)$ submatrix of $R(\hat{p})$, $R_s(\hat{p})$, such that det$[R_s(\hat{p})] \neq 0$. The submatrix $R_s(\hat{p})$ has nonzero elements of the form $(\hat{p}_i - \hat{p}_j)^T$, $(i,j) \in E_I$. From Lemma 2.1, we know that if dist$(\bar{p}, \mathcal{H}(p)) \leq \varepsilon$, we can find δ_{ik} and $\bar{T} \in$ Iso$(\mathbb{R}^2)$ such that $[\bar{p}_i]_k = \left[\bar{T}(p_i)\right]_k + \delta_{ik} = [\hat{p}_i]_k + \delta_{ik}$. Thus, the nonzero elements of $R_s(\bar{p})$ have the form $[\bar{p}_i]_k - [\bar{p}_j]_k = [\hat{p}_i]_k - [\hat{p}_j]_k + \delta_{ik} - \delta_{jk}$, which are continuously dependent on $\hat{p}$. Since the eigenvalues of a matrix depend continuously on its elements [19] and the determinant of a matrix is the product of its eigenvalues, it follows that the determinant continuously depends on the elements of the matrix. Thus, for sufficiently small δ_{ik}, we have that rank$[R_s(\bar{p})]$ = rank$[R_s(\hat{p})] = 2n - 3$ and the framework $\bar{F}$ is infinitesimally rigid. ■

Corollary 2.1 Consider the set

$$\mathcal{I}(p, E) = \left\{\hat{p} \in \mathbb{R}^{2n} \mid \|\hat{p}_i - \hat{p}_j\|_2 = \|p_i - p_j\|_2, (i,j) \in E\right\} \tag{2.17}$$

where E is some edge set. If $F = (G, p)$ is infinitesimally rigid, then so is $\bar{F} = (G, \bar{p})$ if the point $\bar{p}$ is sufficiently close to $\mathcal{I}(p, E_g)$.

Proof. From the definition of global rigidity, we have that $\mathcal{I}(p, E_g) = \mathcal{H}(p)$. ■

Let $\mathcal{A}$ be the set of all flip-ambiguous frameworks equivalent to F_I, then $\mathcal{I}(p, E_I) = \mathcal{I}(p, E_g) \cup \mathcal{A}$. Note that due to (2.6), for any $\bar{p} \in \mathbb{R}^{2n}$,

$$\text{dist}\left(\bar{p}, \mathcal{I}(p, E_I)\right) = \min\left\{\text{dist}\left(\bar{p}, \mathcal{I}(p, E_g)\right), \text{dist}\left(\bar{p}, \mathcal{A}\right)\right\}. \tag{2.18}$$

Also, given the set

$$\Omega(p) = \left\{\hat{p} \in \mathbb{R}^{2n} \mid \text{dist}\left(\hat{p}, \mathcal{I}(p, E_g)\right) \leq \varepsilon\right\}, \tag{2.19}$$

we can always find a sufficiently small ε such that $\forall \bar{p} \in \Omega(p)$,

$$\text{dist}\left(\bar{p}, \mathcal{I}(p, E_g)\right) \leq \text{dist}\left(\bar{p}, \mathcal{A}\right). \tag{2.20}$$

In other words, $\bar{p}$ can be selected to be "closer" to $F_I = (G_I, p)$ than to any flip-ambiguous framework equivalent to F_I.[2]

Lemma 2.3 Let $v \in \mathbb{R}^2$ and $\mathbf{1}_n$ be the $n \times 1$ vector of ones, then $R(p)(\mathbf{1}_n \otimes v) = 0$.

Proof. From (2.3), it is not difficult to see that each row of the rigidity matrix $R(p)$ takes the form

$$\left[0 \ldots 0,\ (p_i - p_j)^T, 0 \ldots 0,\ (p_j - p_i)^T,\ 0\ \ldots\ 0\right]. \tag{2.21}$$

Thus, the dot product of each row of $R(p)$ and the $2n \times 1$ vector $\mathbf{1}_n \otimes v$ will be zero. ■

[2] Recall that F_I was obtained by removing edges from F_g.

Chapter 3 Problem Statement

Consider a system of n agents moving in the plane where $q_i = (x_i, y_i) \in \mathbb{R}^2$ is the position of the ith agent relative to an Earth-fixed coordinate frame, and $u_i \in \mathbb{R}^2$ is the corresponding control input. Note that u_i can be a velocity-, acceleration-, or actuator-level input depending on the mathematical model for the agent motion.

Consider a globally rigid formation in $\mathbb{R}^2$ described by the framework $F_g^* = (G_g^*, q_g^*)$ where $G_g^* = \left(V^*, E_g^*\right)$, $\dim(V^*) = n$, $\dim(E_g^*) = l_g^*$, $q_g^* = \left(q_{g1}^*, \ldots, q_{gn}^*\right)$ is one of the solutions of $\phi_{E_g^*}^{-1}(d_g) \neq \emptyset$, $d_g = (\ldots, d_{ij}, \ldots) \in \mathbb{R}^{l_g^*}$, and $d_{ij} > 0$, $(i,j) \in E_g^*$ is the *constant* desired distance between agents i and j. We arbitrarily remove edges from G_g^* to obtain an infinitesimally and minimally rigid framework $F^* = (G^*, q^*)$ where $G^* = (V^*, E^*)$, $E^* \subseteq E_g^*$, $\dim(E^*) = l^* \leq l_g^*$, $q^* = (q_1^*, \ldots, q_n^*) = q_g^*$. Let F^* represent the *desired formation*.

Consider that the actual formation of the agents is represented by the framework $F(t) = (G^*, q(t))$ where $q = (q_1, \ldots, q_n)$. Assume that at $t = 0$ the agents do not satisfy the desired inter-agent distance constraints, i.e., $\|q_i(0) - q_j(0)\|_2 \neq d_{ij}$, $(i,j) \in E_g^*$.

We deal with three types of control problems for the multi-agent system: formation acquisition, formation maneuvering, and target interception. In formation acquisition, the goal is for the agents to acquire and maintain a pre-defined, fixed geometric shape in the plane. The control objective for formation acquisition, which serves as the *common*, primary objective for the other two problems, can be mathematically described as to design u_i such that

$$\|q_i(t) - q_j(t)\|_2 \to d_{ij} \text{ as } t \to \infty, \ \ (i,j) \in E_g^*. \tag{3.1}$$

In the formation maneuvering problem, agents are required to simultaneously acquire a formation (satisfy (3.1)) and move cohesively following a pre-defined (time-varying) trajectory. Thus, the secondary objective is

$$\dot{q}_i(t) - v_d(t) \to 0 \text{ as } t \to \infty, \ i = 1, ..., n \tag{3.2}$$

where $v_d \in \mathbb{R}^2$ is any bounded, continuous function representing the desired translational velocity for the swarm of agents.

In the target interception problem, the agents should intercept and surround a moving target with a pre-defined formation. To facilitate the solution, we will take the nth agent to be the *leader*

while the remaining agents are followers. Our control protocol will consist of: a) selecting F^* with the additional property that $q_n^* \in \text{conv}\{q_1^*, ..., q_{n-1}^*\}$ where $\text{conv}\{\cdot\}$ denotes the convex hull, b) the leader tracking the target, and c) the followers tracking the leader while maintaining the desired formation. Thus, if $q_T \in \mathbb{R}^2$ denotes the target position, the secondary objective for this problem is that $q_T(t)$ approach $\text{conv}\{q_1(t), q_2(t), ..., q_{n-1}(t)\}$ as $t \to \infty$; i.e., using the notation from [20],

$$q_T(t) \in \text{conv}\{q_1(t), q_2(t), ..., q_{n-1}(t)\} \text{ as } t \to \infty. \tag{3.3}$$

Chapter 4 Single-Integrator Agent Model

Consider that the system of n agents is modeled by the single integrator equation

$$\dot{q}_i = u_i, \quad i = 1, \ldots, n \tag{4.1}$$

where u_i is the velocity-level control input of the ith agent. In this chapter, we will design $u_i = u_i(q_i - q_j, d_{ij})$, $i = 1, \ldots, n$ and $j \in \mathcal{N}_i(E^*)$ where $\mathcal{N}_i(\cdot)$ was defined in (2.1) to achieve the control objectives described by (3.1), (3.2), and (3.3).

4.1 Control Formulation

Define the relative position of two agents as

$$\tilde{q}_{ij} = q_i - q_j, \quad (i,j) \in E^*, \tag{4.2}$$

and let $\tilde{q} = (\ldots, \tilde{q}_{ij}, \ldots) \in \mathbb{R}^{2l}$ with the same ordering of terms as the edge function (2.2). The distance error is given by

$$e_{ij} = \|\tilde{q}_{ij}\|_2 - d_{ij}, \quad (i,j) \in E^*. \tag{4.3}$$

Note that (3.1) is equivalent to $e_{ij}(t) \to 0$ as $t \to \infty$, $(i,j) \in E_g^*$. It follows from (4.3) and (4.1) that the distance error dynamics is

$$\begin{aligned} \dot{e}_{ij} &= \frac{d}{dt}\left(\sqrt{\tilde{q}_{ij}^T \tilde{q}_{ij}}\right) \\ &= \left(\tilde{q}_{ij}^T \tilde{q}_{ij}\right)^{-\frac{1}{2}} \tilde{q}_{ij}^T (u_i - u_j) \\ &= \frac{\tilde{q}_{ij}^T (u_i - u_j)}{e_{ij} + d_{ij}}. \end{aligned} \tag{4.4}$$

Consider the potential function [15, 26, 33]

$$W_{ij} = \frac{1}{4} z_{ij}^2. \tag{4.5}$$

where

$$z_{ij} = \|\tilde{q}_{ij}\|_2^2 - d_{ij}^2, \quad (i,j) \in E^*. \tag{4.6}$$

Note that (4.6) can be rewritten using (4.3) as

$$z_{ij} = e_{ij}\left(\|\tilde{q}_{ij}\|_2 + d_{ij}\right) = e_{ij}\left(e_{ij} + 2d_{ij}\right). \tag{4.7}$$

Since $\|\tilde{q}_{ij}\|_2 \neq -d_{ij}$ because $\|\tilde{q}_{ij}\|_2 \geq 0$ (or equivalently, $e_{ij} \neq -2d_{ij}$ because $e_{ij} \geq -d_{ij}$), it is easy to that $z_{ij} = 0$ if and only if $e_{ij} = 0$. Therefore, (4.5) is positive definite and radially unbounded in e_{ij}.

We now define the following Lyapunov function candidate

$$W(e) = \sum_{(i,j)\in E^*} W_{ij} \tag{4.8}$$

where $e = (\ldots, e_{ij}, \ldots) \in \mathbb{R}^{l^*}$ is ordered as (2.2). The time derivative of (4.8) along (4.4) is given by

$$\dot{W} = \sum_{(i,j)\in E^*} e_{ij}\left(e_{ij} + 2d_{ij}\right)\tilde{q}_{ij}^T\left(u_i - u_j\right). \tag{4.9}$$

It follows from (4.3), (2.3), and (2.2) that (4.9) can be rewritten as[3]

$$\dot{W} = z^T R(q) u \tag{4.10}$$

where $u = (u_1, ..., u_n) \in \mathbb{R}^{2n}$, $z = (..., z_{ij}, ...) \in \mathbb{R}^{l^*}$, $(i,j) \in E^*$. The terms in z are ordered in the same way as in (2.2).

4.1.1 Formation Acquisition

Before stating the main result, we introduce the following lemma.

Lemma 4.1 Given (4.8) and a positive constant ε, then $\text{dist}(q, \mathcal{H}(q^*)) \leq \varepsilon$ implies the existence of bounded level surfaces $W(e) \leq c(\varepsilon)$.

Proof. See Appendix A. ■

The control law for formation acquisition is given in the following theorem.

Theorem 4.1 Given the formation $F(t) = (G^*, q(t))$, let ε be a sufficiently small positive constant and $q \in \Omega(q^*)$ where Ω was defined in (2.19). Let the initial condition of (4.1) be such that $\tilde{q}(0) \in \mathcal{S}$ where $\mathcal{S} = \left\{\tilde{q} \in \mathbb{R}^{2l} \mid W(e) \leq c(\varepsilon)\right\}$ and $c(\varepsilon)$ is a sufficiently small positive constant. Then, the control[4]

$$u = u_a := -k_q R^T(q) z, \tag{4.11}$$

where $k_q > 0$, renders $e = 0$ exponentially stable and ensures that (3.1) is satisfied.

---

[3] Although the argument of the rigidity matrix function is commonly given as q, it is clear from (2.2) that R is dependent on $\tilde{q}$ only, i.e., $R = R(\tilde{q})$.

[4] The variable u_a denotes the formation *acquisition* control term that will appear in all control algorithms developed throughout the dissertation.

Proof. First, since F^* and $F(t)$ have necessarily the same number of edges, the minimal rigidity of F^* implies that $F(t)$ is minimally rigid for all $t \geq 0$.

Since $q \in \Omega(q^*)$ with sufficiently small ε, it follows from (2.19) and (2.20) that

$$\min\left\{\text{dist}\left(q, \mathcal{I}\left(q^*, E_g^*\right)\right), \text{dist}\left(q, \mathcal{A}^*\right)\right\} = \text{dist}\left(q, \mathcal{I}\left(q^*, E_g^*\right)\right) \tag{4.12}$$

where $\mathcal{I}$ was defined in (2.17) and $\mathcal{A}^*$ is the set of all flip-ambiguous frameworks equivalent to F^*. Thus, from (2.18), we know that $\text{dist}(q, \mathcal{I}(q^*, E^*)) = \text{dist}\big(q, \mathcal{I}\left(q^*, E_g^*\right)\big) \leq \varepsilon$. From Corollary 2.1, we then know that $F = (G^*, q)$ is infinitesimally rigid for $\text{dist}(q, \mathcal{I}(q^*, E^*)) \leq \varepsilon$. From the fact that $\mathcal{I}\left(q^*, E_g^*\right) = \mathcal{H}(q^*)$ (see the proof of Corollary 2.1), we then know $\text{dist}(q, \mathcal{H}(q^*)) \leq \varepsilon$. Therefore, we can use Lemma 4.1 to show that $\text{dist}(q, \mathcal{I}(q^*, E^*)) \leq \varepsilon$ implies the existence of bounded level surfaces $W(e) \leq c(\varepsilon)$. Now, substituting (4.11) into (4.10) yields

$$\dot{W} = -k_q z^T R(q) R^T(q) z. \tag{4.13}$$

Since F is infinitesimally and minimally rigid for $\tilde{q} \in \mathcal{S}$, then $R(q)$ has full row rank. Since $\text{rank}[R(q)] = \text{rank}\big[R(q) R^T(q)\big]$, the matrix $R(q) R^T(q)$ is invertible for $\tilde{q} \in \mathcal{S}$; therefore,

$$\dot{W} \leq -k_q \lambda_{\min}\left(RR^T\right) z^T z = -4k_q \lambda_{\min}\left(RR^T\right) W \tag{4.14}$$

for $\tilde{q}(t) \in \mathcal{S}$, where $\lambda_{\min}(\cdot)$ denotes the minimum eigenvalue. Since $\dot{W}$ is negative definite, the level surfaces of W are invariant [24] and, if $\tilde{q}(0) \in \mathcal{S}$, $\tilde{q}(t)$ stays in $\mathcal{S}$ for all $t > 0$. Thus, from the form of (4.14), $e = 0$ is exponentially stable for $\tilde{q}(0) \in \mathcal{S}$ [24]. Since $F(t)$ is infinitesimally rigid for $t \geq 0$ and flip ambiguities have been avoided, the exponential stability of $e = 0$ implies that $\|\tilde{q}_{ij}(t)\|_2 \to d_{ij}$ as $t \to \infty$ for all $(i, j) \in E_g^*$. ■

Remark 4.1 Theorem 4.1 implies that the actual formation $F(t)$ needs to be sufficiently close to F_g^* at $t = 0$ to avoid a flip ambiguity while remaining infinitesimally rigid. The control however is only dependent on F^* and $(i, j) \in E^*$. That is, global rigidity of the desired formation is not needed by the control and is only used to properly initialize the system.

Remark 4.2 Some practical implications of the requirements in Theorem 4.1 are that two or more agents cannot be initially collocated, or three or more agents cannot be initially collinear. In either of these situations, $\text{rank}[R(\tilde{q})] < l^*$ so $\dot{W}$ would not necessarily be negative definite.

In fact, rank$[R(\tilde{q}(0))] = l^*$ is a necessary condition for $\tilde{q}(0) \in \mathcal{S}$. Because of these facts, the stability of formation controllers based on rigid graph theory is always local in nature; see, e.g., [14, 26, 33, 44].

Remark 4.3 The control (4.11) can be expressed component-wise as

$$u_i = -k_q \sum_{j \in \mathcal{N}_i(E^*)} \tilde{q}_{ij} z_{ij}, \tag{4.15}$$

It is easy to see from (4.15) that u_i is decentralized in the sense that it only requires the ith agent to measure the relative position w.r.t. its neighbors $\mathcal{N}_i(E^*)$.

4.1.2 Formation Maneuvering

The control law for formation maneuvering is given in the following theorem

Theorem 4.2 Let the initial condition of (4.1) be such that $\tilde{q}(0) \in \mathcal{S}$ where $\mathcal{S}$ was defined in Theorem 4.1. Then, the control

$$u = u_a + (\mathbf{1}_n \otimes v_d), \tag{4.16}$$

where u_a was defined in (4.11) and v_d was defined in (3.2), renders $e = 0$ exponentially stable and ensures that (3.1) and (3.2) are satisfied.

Proof. Following the proof of Theorem 4.1, we substitute (4.16) into (4.10) and apply Lemma 2.3 to yield (4.13). Therefore, $e = 0$ is exponentially stable and (3.1) holds.

Now, from (4.7), it is clear that $z \to 0$ as $e \to 0$. Therefore, since $R(q)$ is bounded from the above stability result, we have that $u \to (\mathbf{1}_n \otimes v_d)$ as $e \to 0$. Since we have proven that $e(t) \to 0$ as $t \to \infty$, it follows from (4.1) that $\dot{q}_i(t) - v_d(t) \to 0$ as $t \to \infty$, $i = 1, ..., n$. ■

Remark 4.4 The control (4.16) can be thought of as having two independent components: u_a is responsible for formation acquisition while the second term guarantees formation maneuvering. The control law can be expressed component-wise as

$$u_i = -k_q \sum_{j \in \mathcal{N}_i(E^*)} \tilde{q}_{ij} z_{ij} + v_d, \tag{4.17}$$

which shows that the ith agent is only required to measure the relative position w.r.t. its neighbors $\mathcal{N}_i(E^*)$ in addition to knowing the swarm velocity v_d.

4.1.3 Target Interception with Unknown Target Velocity

Here, we assume the leader (i.e., nth agent) can measure the target's relative position $q_T - q_n$ and can broadcast this information to the followers. Given $v_T := \dot{q}_T$, we assume v_T is ***unknown***. We also assume that q_T, v_T, $\dot{v}_T$ and $\ddot{v}_T$ are bounded and continuous; i.e., we assume $q_T(t)$ is three-times continuously differentiable and $d^i q_T/dt^i$, $i = 0, 1, 2, 3$ are bounded. Our control will include the following continuous term to "estimate" the target's unknown velocity [46]

$$\hat{v}_T(t) = \int_0^t \left[k_1 e_T(\tau) + k_2 \text{sgn}\left(e_T(\tau)\right)\right] d\tau \tag{4.18}$$

where

$$e_T = q_T - q_n \tag{4.19}$$

denotes the interception error between the leader and target, $k_1, k_2 > 0$, $\text{sgn}(x) = (sgn(x_1), \ldots, sgn(x_n))\ \forall x \in \mathbb{R}^n$, and $sgn(\cdot)$ is the standard signum function, i.e.,

$$sgn(x_i) = \begin{cases} 1 & \text{for } x_i > 0 \\ 0 & \text{for } x_i = 0 \\ -1 & \text{for } x_i < 0. \end{cases} \tag{4.20}$$

Before presenting the main result of this section, a lemma modified from its original version in [46] is introduced.

Lemma 4.2 Let

$$L := \left(k_1 e_T + \dot{e}_T\right)^T \left(\dot{v}_T - k_2 \text{sgn}\left(e_T\right)\right). \tag{4.21}$$

If k_2 is selected to satisfy the following sufficient condition

$$k_2 > \|\dot{v}_T\|_{\mathcal{L}_\infty} + \frac{1}{k_1}\|\ddot{v}_T\|_{\mathcal{L}_\infty}, \tag{4.22}$$

where $\|x\|_{\mathcal{L}_\infty} = \sup_{t \geq 0} \|x(t)\|_2$ for any piecewise continuous, bounded functions $x : [0, \infty] \to \mathbb{R}^n$, then

$$\int_0^t L(\tau)\, d\tau \leq \zeta_b \tag{4.23}$$

where the positive constant ζ_b is defined as

$$\zeta_b = k_2 \left\| e_T(0) \right\|_1 - e_T^T(0)\, \dot{v}_T(0) \tag{4.24}$$

and $\|\cdot\|_1$ denotes the vector 1-norm.

Proof. See Appendix B. ■

Theorem 4.3 Let the initial condition of (4.1) be such that $\tilde{q}(0) \in \mathcal{S}$ where $\mathcal{S}$ is defined in Theorem 4.1. Then, the control

$$u = u_a + h_s, \tag{4.25}$$

where

$$h_s = \mathbf{1}_n \otimes \left[(k_1 + 1)\, e_T + \hat{v}_T - u_{an} \right], \tag{4.26}$$

$u_a = (u_{a1}, \ldots, u_{an})$ was defined in (4.11), and $\hat{v}_T(t)$ was defined in (4.18), renders $e = 0$ exponentially stable and ensures that (3.1) and (3.3) are satisfied.

Proof. The proof of Theorem 4.2 can be followed to show that, for $\tilde{q}(0) \in \mathcal{S}$, (4.25) ensures $e = 0$ is exponentially stable and (3.1) holds.

Now, note from (4.25) and (4.26) that[5]

$$u_n = (k_1 + 1)\, e_T + \hat{v}_T. \tag{4.27}$$

Differentiating (4.19) and applying (4.27) yields

$$\dot{e}_T = v_T - u_n = v_T - (k_1 + 1)\, e_T - \hat{v}_T(t) = -k_1 e_T + w \tag{4.28}$$

where

$$w = v_T - e_T - \hat{v}_T. \tag{4.29}$$

After taking the derivative of (4.29), we obtain

$$\dot{w} = \dot{v}_T - \dot{e}_T - k_1 e_T - k_2 \text{sgn}(e_T) = -w + \dot{v}_T - k_2 \text{sgn}(e_T) \tag{4.30}$$

where (4.18) and (4.28) were used.

Next, define the auxiliary function

$$P = \frac{1}{2} w^T w, \tag{4.31}$$

[5] The introduction of the term $-u_{an}$ in (4.26) is crucial for the following stability analysis of the target tracking error since it allows u_n (leader control input) to have the simple form in (4.27).

whose derivative along (4.30) and (4.21) is given by

$$\begin{aligned}\dot{P} &= w^T\left(-w+\dot{v}_T-k_2\text{sgn}\left(e_T\right)\right)\\ &= -w^Tw+L. \end{aligned} \tag{4.32}$$

After integrating both sides of (4.32) with respect to time and applying Lemma 4.2, we obtain

$$\begin{aligned}\int_0^t \dot{P}\left(\tau\right)d\tau &= P\left(t\right)-P\left(0\right)=-\int_0^t w^T\left(\tau\right)w\left(\tau\right)d\tau+\int_0^t L\left(\tau\right)d\tau\\ &\leq -\int_0^t w^T\left(\tau\right)w\left(\tau\right)d\tau+\zeta_b\leq\zeta_b. \end{aligned} \tag{4.33}$$

Since $P\left(0\right)$ is bounded, it follows from (4.33) that $P\left(t\right)\in\mathcal{L}_\infty$ [24], which implies that $w(t)\in\mathcal{L}_\infty$ from (4.31). It also follows from (4.33) that

$$\int_0^t w^T\left(\tau\right)w\left(\tau\right)d\tau\leq\zeta_b+P\left(0\right)-P\left(t\right)<\infty,$$

which means that $w\left(t\right)\in\mathcal{L}_2$ [24]. Therefore, we know from (4.28) that $e_T(t)\rightarrow 0$ as $t\rightarrow\infty$ (see Theorem 2.13 in [31]). It can also be shown from (4.28) that $\dot{e}_T\in\mathcal{L}_\infty$, which implies (together with the boundedness of $v_T(t)$) that $u_n(t)\in\mathcal{L}_\infty$. From (4.27), we then know that $\hat{v}_T(t)\in\mathcal{L}_\infty$.

Finally, since we know (4.25) ensures $q_n(t)\in\text{conv}\{q_1(t),q_2(t),...,q_{n-1}(t)\}$ as $t\rightarrow\infty$ due to the manner in which F^* is constructed, we can conclude from the fact that $e_T(t)\rightarrow 0$ as $t\rightarrow\infty$ that (3.3) holds. ■

Remark 4.5 Similar to the formation maneuvering control, the target interception controller (4.25) and (4.26) has two components with well defined roles: the term u_a ensures formation acquisition while the term h_s guarantees target interception. The controller can be written componentwise as

$$u_i=-k_q\sum_{j\in\mathcal{N}_i(E^*)}\tilde{q}_{ij}z_{ij}+\left(\left(k_1+1\right)e_T+\int_0^t\left[k_1e_T\left(\tau\right)+k_2\text{sgn}\left(e_T\left(\tau\right)\right)\right]d\tau-u_{an}\right); \tag{4.34}$$

i.e., the ith control input depends on the relative position w.r.t. its neighbors $\mathcal{N}_i\left(E^*\right)$, the target interception error, and the formation acquisition control term of the leader.

Remark 4.6 Note that target interception error (4.19) could be redefined to include a constant offset so the leader does not end up "on top" of the target, i.e., $e_T=q_n-q_T-\epsilon$ where $\epsilon\in\mathbb{R}^2$ with h_s in (4.26) being redefined accordingly.

4.2 Simulation Results

In this section, MATLAB simulations are presented demonstrating the performance of the above-designed controllers.

4.2.1 Formation Acquisition

A five-agent simulation was conducted to show that control objective (3.1) is achieved by applying control input (4.11) to (4.1). The desired formation was the regular convex pentagon shown in Figure 4.1 with vertices at $(0,1)$, $(-s_1,c_1)$, $(-s_2,-c_2)$, $(s_2,-c_2)$, (s_1,c_1) where $s_1 = \sin 2\pi/5$, $s_2 = \sin 4\pi/5$, $c_1 = \cos 2\pi/5$, $c_2 = \cos \pi/5$. The vertices were ordered counterclockwise with the coordinate $(0,1)$ as vertex number 1 (i.e., $q_1^* = (0,1)$). The desired framework was made minimally rigid and infinitesimally rigid by introducing seven edges and leaving the vertex pairs 2-5, 2-4, and 3-5 disconnected. Thus, given the edge ordering shown in Figure 4.1, the desired distance vector was set to $d = (d_{12}, d_{13}, d_{14}, d_{15}, d_{23}, d_{34}, d_{45})$ where $d_{12} = d_{23} = d_{34} = d_{45} = d_{15} = \sqrt{2(1-c_1)}$ and $d_{13} = d_{14} = \sqrt{2\,(1+c_2)}$.

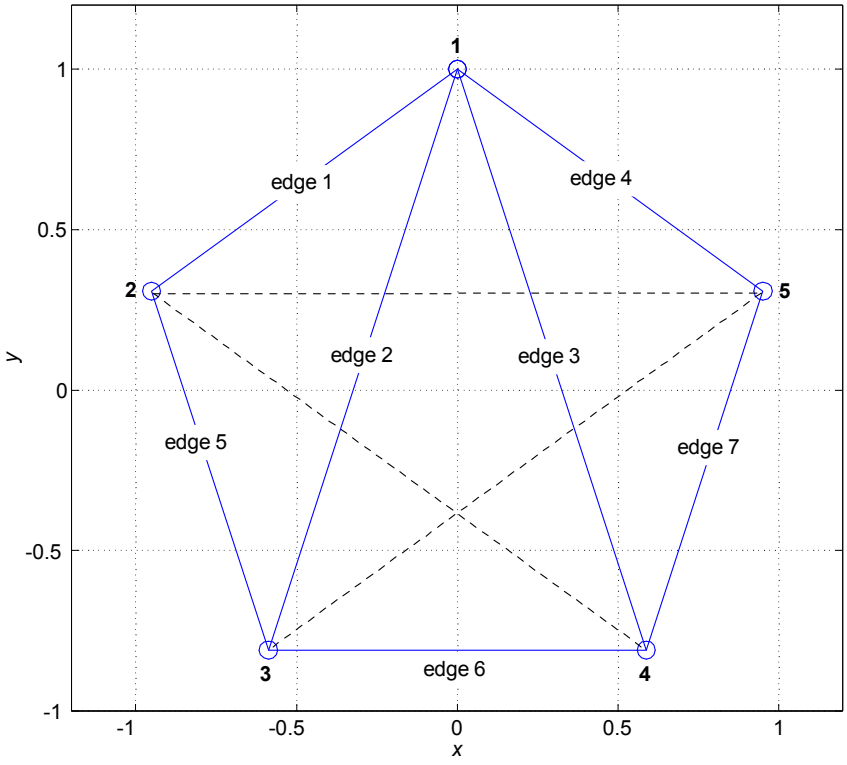

Figure 4.1: Desired formation for five agents.

The initial conditions of the agents were selected by

$$q_i(0) = q_i^* + \delta\left[\text{rand}(0,1) - 0.5\mathbf{1}_2\right], \quad i = 1, \ldots, 5 \tag{4.35}$$

where $\delta = 1$, $\mathbf{1}_2$ is the 2×1 vector of ones, and $\text{rand}(0,1)$ generates a random 2×1 vector whose elements are uniformly distributed on the interval $(0,1)$. The control gain k_q was set to 1. Figure 4.2 shows the trajectories of the five agents forming the desired shape (up to rotation and translation), while Figure 4.3 shows the distance errors $e_{ij}(t)$, $i, j \in V^*$ approaching zero. The x- and y-direction components of the control inputs $u_i(t)$, $i = 1, \ldots, 5$ are given in Figure 4.4.

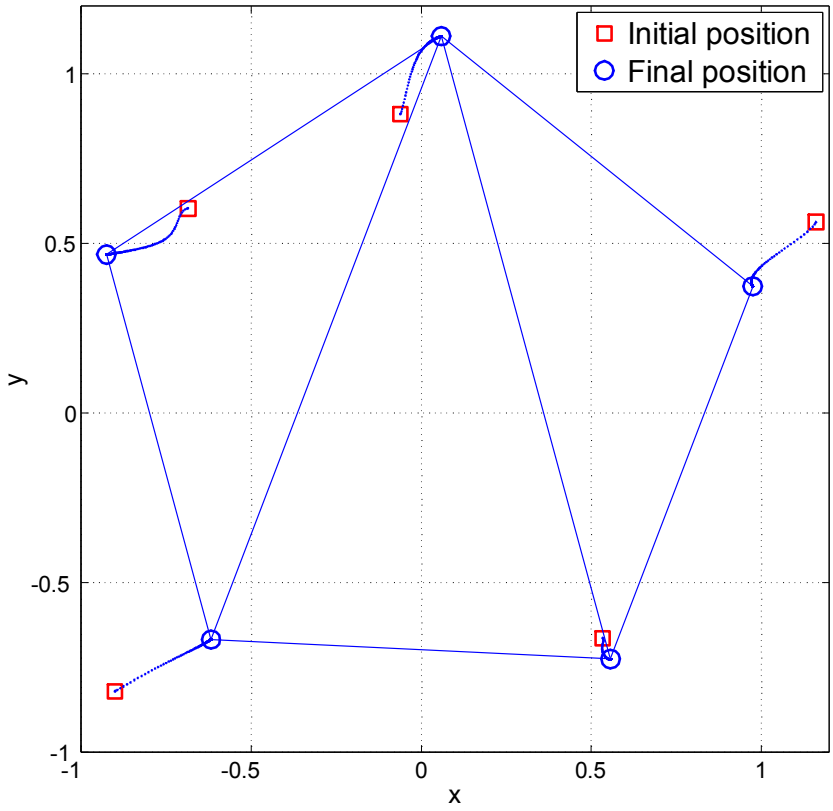

Figure 4.2: Single-integrator formation acquisition: agent trajectories $q_i(t)$, $i = 1, ..., 5$.

A second simulation was conducted to demonstrate the local nature of the stability result. To this end, the distance between each agent at $t = 0$ and the corresponding target position was increased by selecting the initial conditions according to (4.35) with $\delta = 2$. The simulation results in Figure 4.5 show the agents reaching an incorrect formation, which is likely due to $\tilde{q}(0) \notin \mathcal{S}$. In fact, notice that this incorrect formation corresponds to a graph where edges 4 and 7 are flipped over edge 3 (see labels in Figure 4.1). That is, in this case, the control drives the agents to a formation

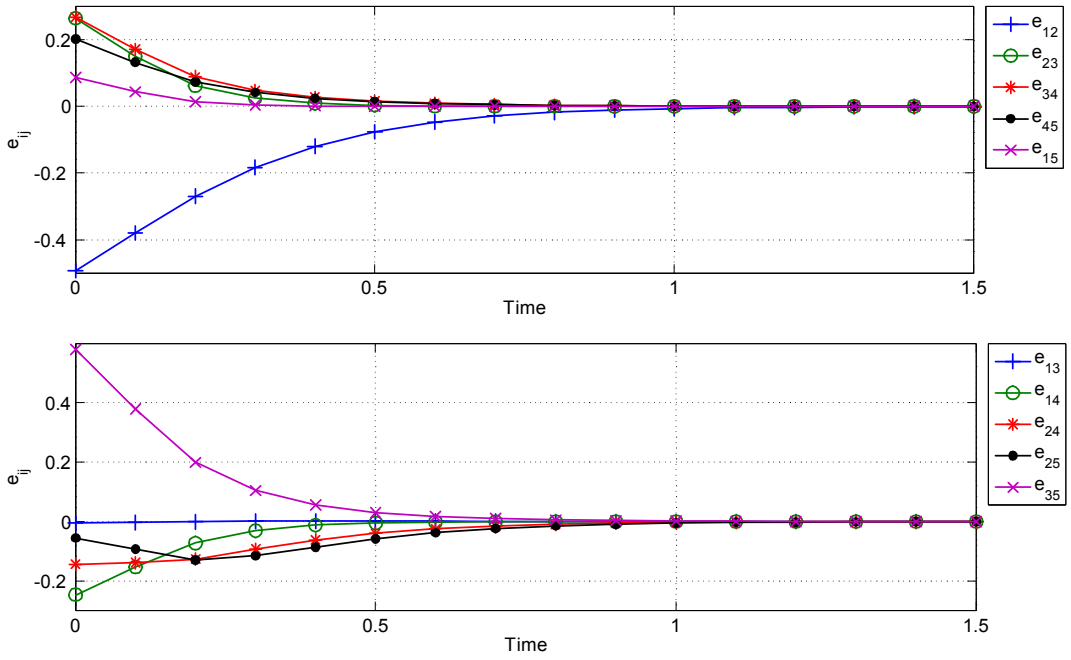

Figure 4.3: Single-integrator formation acquisition: distance errors $e_{ij}(t)$, $i, j \in V^*$.

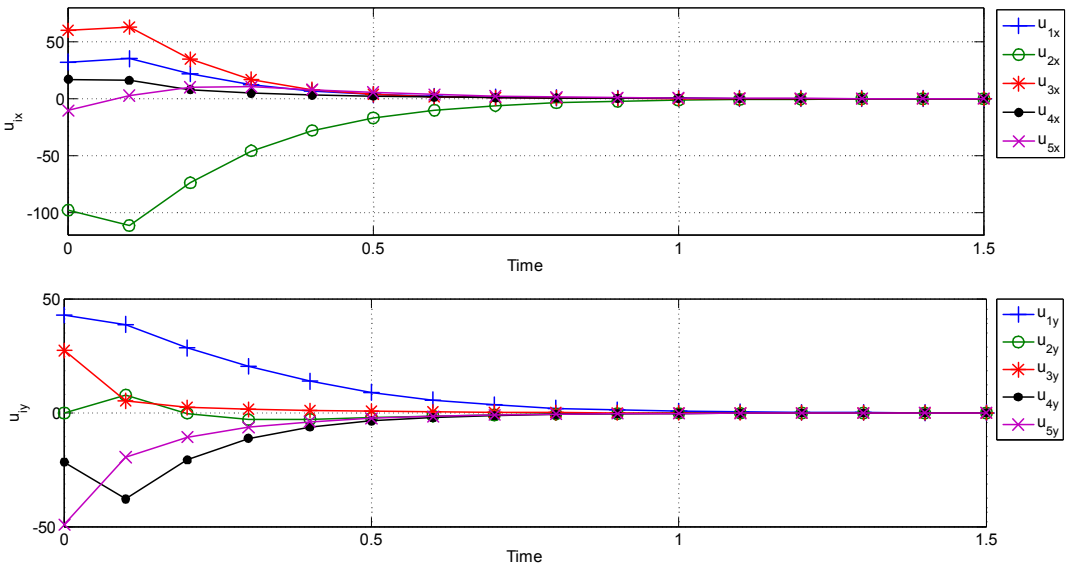

Figure 4.4: Single-integrator formation acquisition: control inputs $u_i(t)$ $i = 1, \ldots, 5$.

with the desired edge lengths *only* for agent pairs $(i,j) \in E^*$. Convergence to the desired edge lengths for all agent pairs $(i,j) \in E_g^*$ only occurs if the agents are sufficiently close to F_g^* (the globally rigid framework associated with Figure 4.1) at $t = 0$.

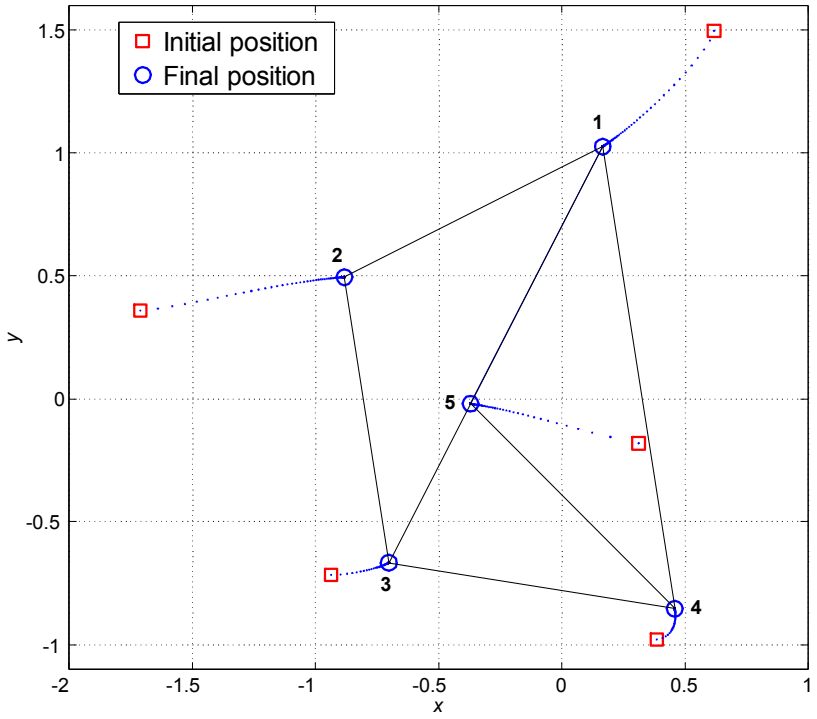

Figure 4.5: Single-integrator formation acquisition: agent trajectories for initial conditions outside local stability set.

Now, given the same initial conditions in Figure 4.5, if instead of selecting the graph as in Figure 4.1, we choose the edges to be $(1,2)$, $(2,3)$, $(3,4)$, $(4,5)$, $(1,5)$, $(2,4)$, and $(2,5)$, leaving the vertex pairs $(1,3)$, $(1,4)$, and $(3,5)$ disconnected, the agents converge to the desired formation as shown in Figure 4.6. This suggests that the edges of the desired framework could be chosen according to the actual formation at $t = 0$ to avoid convergence to a flip formation.

4.2.2 Formation Maneuvering

The desired formation for this simulation was the same as in Figure 4.1. The desired swarm velocity v_d was set to

$$v_d = (1, \cos t)\,. \tag{4.36}$$

The initial conditions of the agents were selected by (4.35) with δ set to 1. The control gain k_q in (4.16) was set to 0.3.

Figure 4.7 shows the agent trajectories over time as they acquire and maintain the desired formation, while translating according to (4.36). Figure 4.8 shows the inter-agent distance errors $e_{ij}(t)$, $i, j \in V^*$ approaching zero. The x- and y-direction components of the control inputs $u_i(t)$, $i = 1, \ldots, 5$ are given in Figure 4.9. Notice that in the x (resp., y) direction, the control input converges to the first (resp., second) element of (4.36).

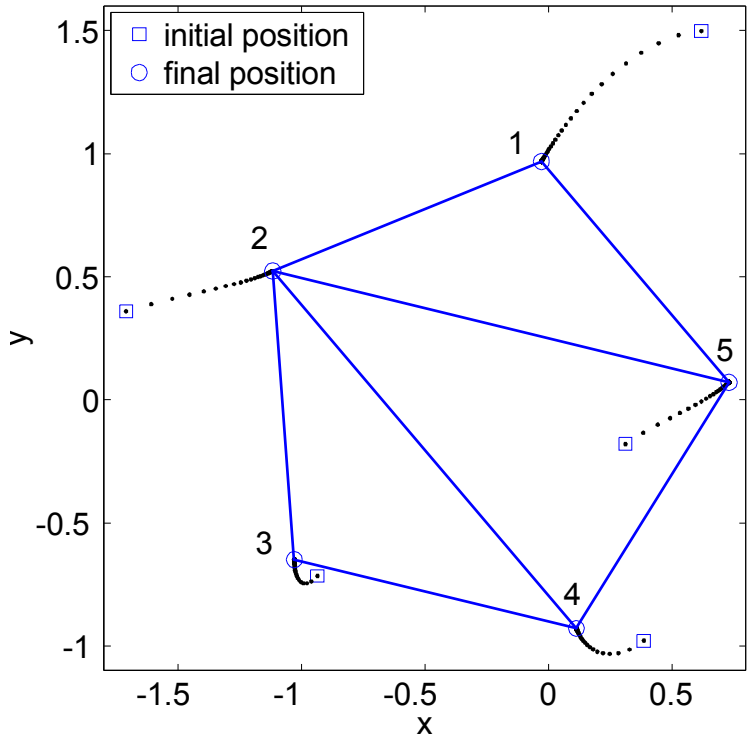

Figure 4.6: Single-integrator formation acquisition: converge to desired formation after changing the graph edges.

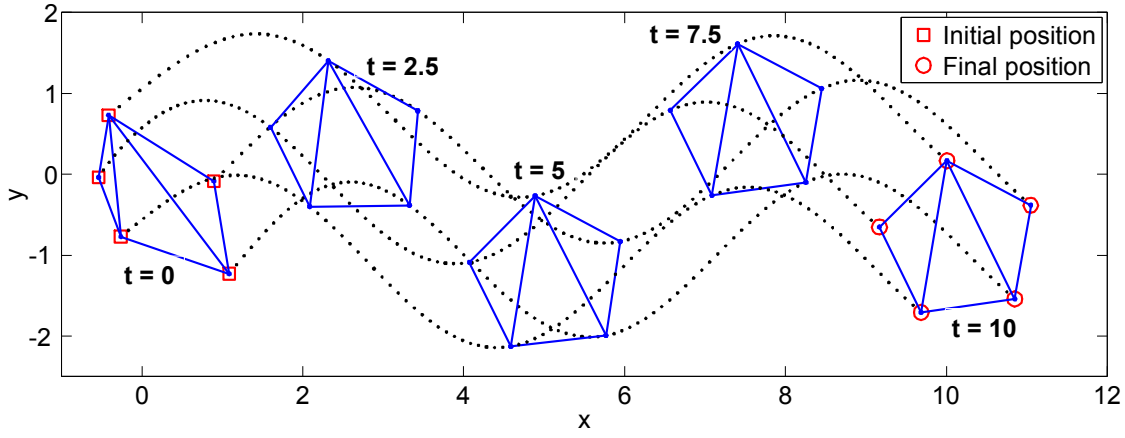

Figure 4.7: Single-integrator formation maneuvering: agent trajectories.

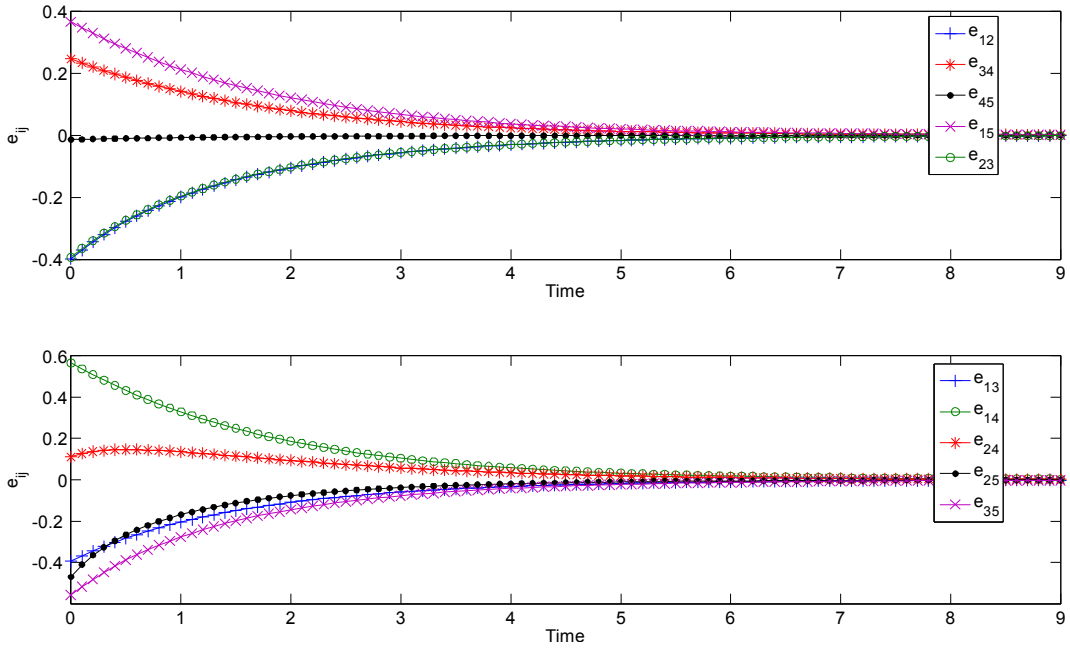

Figure 4.8: Single-integrator formation maneuvering: inter-agent distance errors for $i, j \in V^*$.

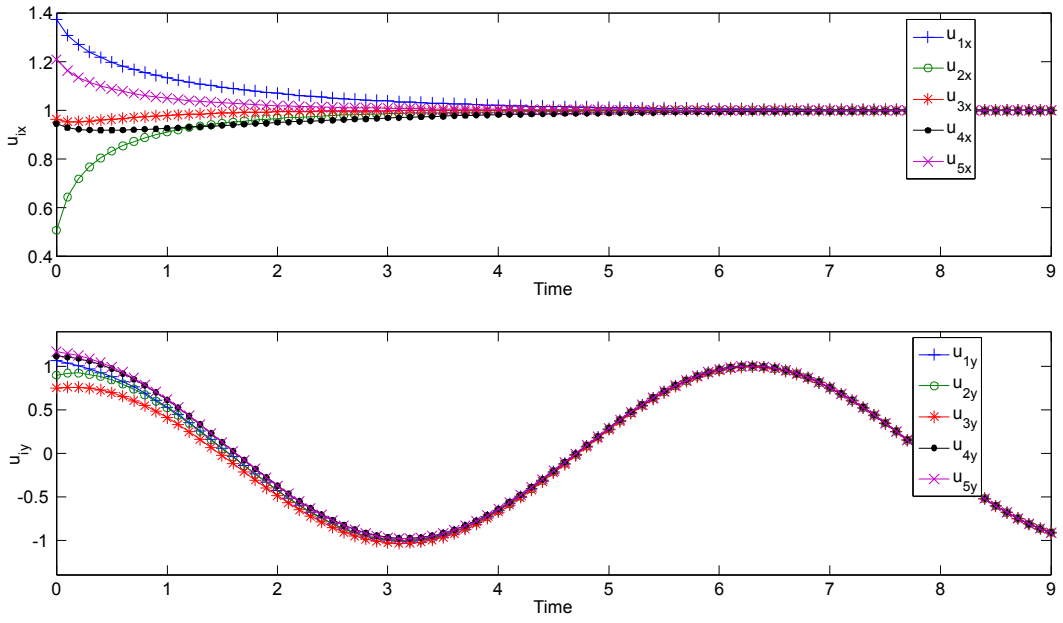

Figure 4.9: Single-integrator formation maneuvering: control inputs along x and y directions.

4.2.3 Target Interception

This simulation was conducted with six agents (one leader and five followers) plus the moving target, whose velocity was set to

$$v_T = (1, \cos t) \tag{4.37}$$

with initial position $q_T(0) = (2, 0)$. The desired formation was the regular convex pentagon with the leader (agent 6) located at the origin; see Figure 4.10. The desired framework was made minimally rigid and infinitesimally rigid by introducing nine edges and leaving vertex pairs $(1, 3)$, $(1, 4)$, $(2, 4)$, $(2, 5)$, $(3, 5)$, and $(5, 6)$ disconnected. Given the edge ordering in Figure 4.10, we have the edge set $E^* = \{(1, 2), (1, 5), (1, 6), (2, 3), (2, 6), (3, 4), (3, 6), (4, 5), (4, 6)\}$. The desired distances between all the agents were given by $d_{12} = d_{23} = d_{34} = d_{45} = d_{15} = \sqrt{2(1 - c_1)}$, $d_{13} = d_{14} = d_{24} = d_{25} = d_{35} = \sqrt{2(1 + c_2)}$, and $d_{16} = d_{26} = d_{36} = d_{46} = d_{56} = 1$.

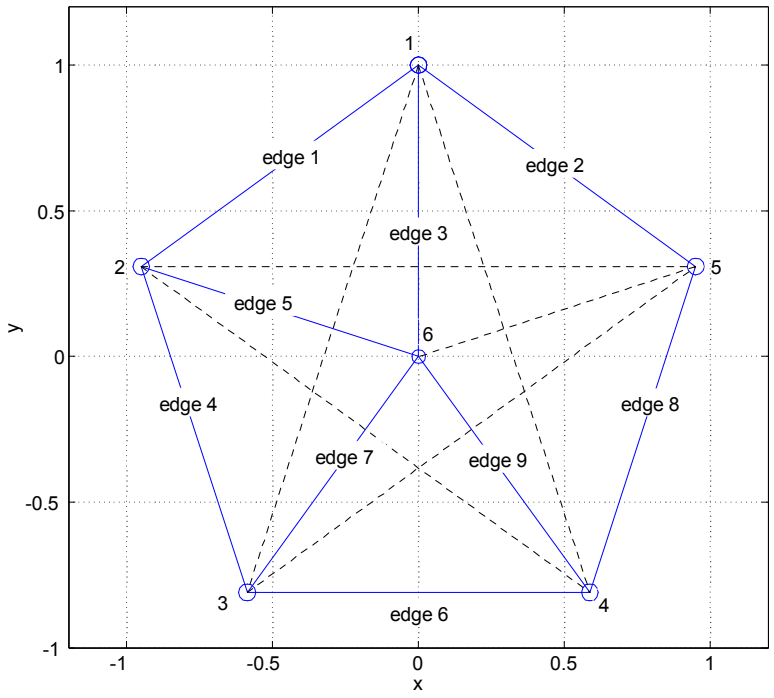

Figure 4.10: Target interception: desired framework.

The initial conditions were again set by (4.35) with $i = 1, ..., 6$ while $\hat{v}_T(0) = 0$. The control gains in (4.25) and (4.26) were set to $k_q = 0.3$, $k_1 = 2$, and $k_2 = 2$. The value for k_2 is in accordance with the inequality (4.22) since, from (4.37), we have $\|\dot{v}_T\|_{\mathcal{L}_\infty} = \|\ddot{v}_T\|_{\mathcal{L}_\infty} = 1$. Figures 4.11 and 4.12 show that the control objectives were successfully met. Figure 4.13 shows the control inputs of each agent converging to v_T, despite the target velocity being unknown.

We note that very similar results were obtained with $k_2 = 1$, which does not satisfy (4.22). This demonstrates that (4.22) is indeed only a *sufficient* condition for stability of the target tracking error.

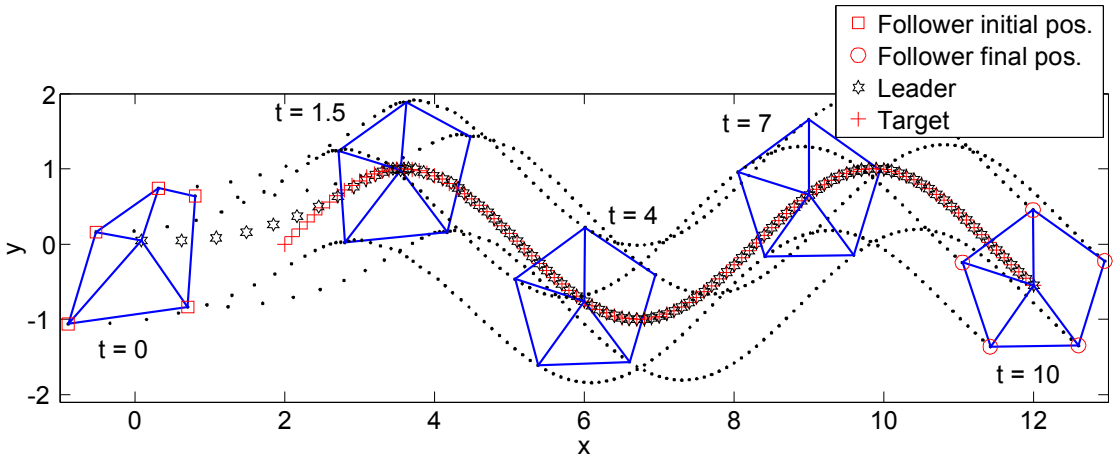

Figure 4.11: Single-integrator target interception with unknown target velocity: target and agents trajectory.

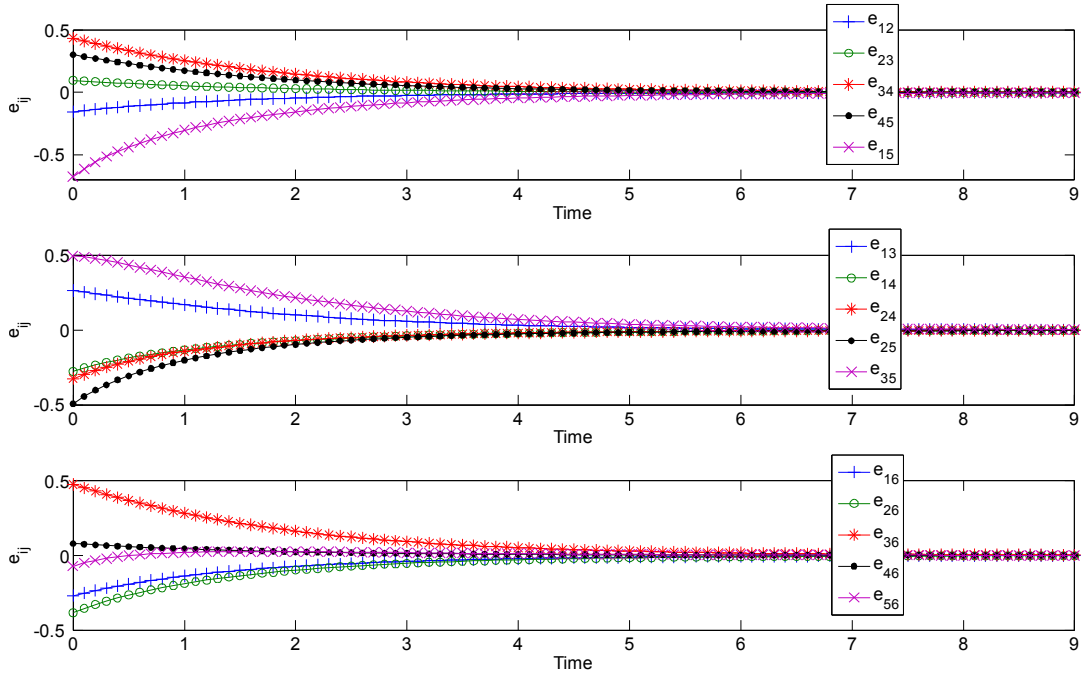

Figure 4.12: Single-integrator target interception with unknown target velocity: inter-agent distance errors for $i, j \in V^*$.

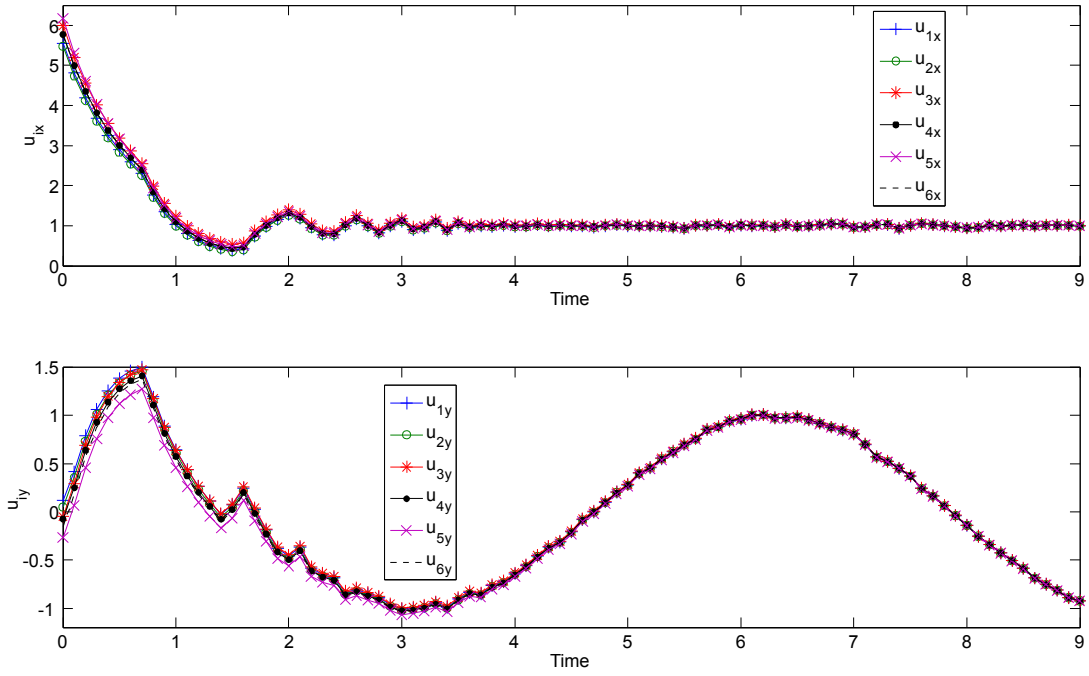

Figure 4.13: Single-integrator target interception with unknown target velocity: control inputs along x and y direction.

Chapter 5 Double-Integrator Agent Model

In this chapter, we consider that the motion of the multi-agent system is modeled by the double integrator

$$\dot{q}_i = v_i \tag{5.1a}$$

$$\dot{v}_i = u_i, \quad i = 1, \ldots, n \tag{5.1b}$$

where $v_i, u_i \in \mathbb{R}^2$ represent the velocity and acceleration-level control input of the ith agent, respectively. We will design $u_i = u_i(q_i - q_j, v_i - v_j, v_i, d_{ij})$, $i = 1, \ldots, n$ and $j \in \mathcal{N}_i(E^*)$ where $\mathcal{N}_i(\cdot)$ was defined in (2.1) to achieve the same control objectives as the previous chapter, i.e., (3.1), (3.2), and (3.3).

5.1 Control Formulation

From (4.3) and (5.1a), the distance error dynamics is written as

$$\begin{aligned} \dot{e}_{ij} &= \frac{d}{dt}\left(\sqrt{\tilde{q}_{ij}^T \tilde{q}_{ij}}\right) \\ &= \left(\tilde{q}_{ij}^T \tilde{q}_{ij}\right)^{-\frac{1}{2}} \tilde{q}_{ij}^T \left(v_i - v_j\right) \\ &= \frac{\tilde{q}_{ij}^T \left(v_i - v_j\right)}{e_{ij} + d_{ij}}. \end{aligned} \tag{5.2}$$

Consider the potential function defined in (4.5) and (4.8). Its time derivative along (5.2) is given by

$$\dot{W} = \sum_{(i,j)\in E^*} e_{ij}\left(e_{ij} + 2d_{ij}\right)\tilde{q}_{ij}^T\left(v_i - v_j\right). \tag{5.3}$$

It follows from (4.3), (2.3), and (2.2) that (5.3) can be rewritten as

$$\dot{W} = z^T R(q) v \tag{5.4}$$

where $v = (v_1, ..., v_n) \in \mathbb{R}^{2n}$ and z was defined in (4.10).

Following the backstepping technique [27], we introduce the variable

$$s = v - v_f \tag{5.5}$$

where $v_f \in \mathbb{R}^{2n}$ denotes the fictitious velocity input. We also introduce the function

$$W_d(e, s) = W(e) + \frac{1}{2} s^T s \tag{5.6}$$

where W was defined in (4.8). After taking the time derivative of (5.6), we obtain

$$\begin{aligned}\dot{W}_d &= z^T R(q) v + s^T \dot{s} \\ &= z^T R(q) \left(s + v_f\right) + s^T \left(u - \dot{v}_f\right) \\ &= z^T R(q) v_f + s^T \left[u + R^T \left(q\right) z - \dot{v}_f\right] \end{aligned} \tag{5.7}$$

where (5.4), (5.1b), and (5.5) were used, and $u = (u_1, ..., u_n) \in \mathbb{R}^{2n}$.

5.1.1 Formation Acquisition

The following theorem gives the main result of formation acquisition controller for the double-integrator model.

Theorem 5.1 Let the initial condition of (5.1) be such that $(\tilde{q}(0), v(0)) \in \mathcal{S} \times \mathbb{R}^{2n}$ where $\mathcal{S}$ is defined in Theorem 4.1. Then, the control

$$u = -k_v s + \dot{v}_f - R^T \left(q\right) z, \tag{5.8}$$

where

$$v_f = u_a, \tag{5.9}$$

u_a was defined in (4.11) and $k_v > 0$, renders $(e, s) = 0$ exponentially stable and ensures that (3.1) is satisfied.

Proof. Following the proof of Theorem 4.1, we can show the existence of a bounded level set $W(e) \leq c(\varepsilon)$. Now, substituting (5.8) and (5.9) into (5.6) yields

$$\dot{W}_d = -k_q z^T R \left(q\right) R^T \left(q\right) z - k_v s^T s. \tag{5.10}$$

Since F is infinitesimally and minimally rigid for $\tilde{q} \in \mathcal{S}$, then $R\left(q\right)$ has full row rank and $R\left(q\right) R^T \left(q\right)$ is invertible for $\tilde{q} \in \mathcal{S}$; therefore,

$$\begin{aligned}\dot{W}_d &\leq -k_q \lambda_{\min} \left(R \left(q\right) R^T \left(q\right)\right) z^T z - k_v s^T s \\ &\leq -\min \left\{2k_v, 4k_q \lambda_{\min} \left(R R^T\right)\right\} W_d \end{aligned} \tag{5.11}$$

for $(\tilde{q}(t), v(t)) \in \mathcal{S} \times \mathbb{R}^{2n}$, where $\lambda_{\min}\left(\cdot\right)$ denotes the minimum eigenvalue and W_d was defined in (5.6). Since (5.11) is negative definite, the level sets of W_d are invariant [24] and, if $\tilde{q}(0) \in \mathcal{S}$, $\tilde{q}(t)$ stays in $\mathcal{S}$ for all $t > 0$. Thus, from the form of (5.11), $(e, s) = 0$ is exponentially stable for

$(\tilde{q}(0), v(0)) \in \mathcal{S}\times\mathbb{R}^{2n}$ [24]. Finally, since $F(t)$ is infinitesimally rigid $\forall t \geq 0$ and flip ambiguities have been avoided, the exponential stability of $(e, s) = 0$ implies that $\|q_i(t) - q_j(t)\|_2 \to d_{ij}$ as $t \to \infty$ for all $(i, j) \in E_g^*$. ■

Remark 5.1 The expression for $\dot{v}_f$ in (5.9) is given by

$$\dot{v}_f = -k_q \dot{R}^T z - k_q R^T \dot{z} \tag{5.12}$$

where from (2.3)

$$\dot{R} = R\,(v)\,, \tag{5.13}$$

and from (4.7) and (5.4)

$$\dot{z} = 2R(q)v. \tag{5.14}$$

Remark 5.2 The control (5.8) and (5.9) can be written component-wise as follows

$$u_i = -k_v v_i - \sum_{j\in\mathcal{N}_i(E^*)} \left[(k_v k_q + 1)\,\tilde{q}_{ij} z_{ij} + k_q \left(z_{ij} I_2 + 2\tilde{q}_{ij}\tilde{q}_{ij}^T\right)\tilde{v}_{ij}\right] \tag{5.15}$$

where I_2 is the 2×2 identity matrix and $\tilde{v}_{ij} = v_i - v_j$, $(i, j) \in E^*$. The above control is decentralized in the sense that its implementation only requires each agent to measure its own velocity and the relative position/velocity to its neighbors $\mathcal{N}_i\,(E^*)$.

5.1.2 Formation Maneuvering

The control law for formation maneuvering is given in the following theorem.

Theorem 5.2 Let the initial condition of (5.1) be such that $(\tilde{q}(0), v(0)) \in \mathcal{S}\times\mathbb{R}^{2n}$ where $\mathcal{S}$ is defined in Theorem 4.1. Then, the control (5.8) with

$$v_f = u_a + (\mathbf{1}_n \otimes v_d)\,, \tag{5.16}$$

where u_a and v_d were defined in (4.11) and (3.2), respectively, renders $(e, s) = 0$ exponentially stable and ensures that (3.1) and (3.2) are satisfied.

Proof. After substituting (5.8) and (5.16) into (5.7) and applying Lemma 2.3, we obtain the same

$\dot{W}_d$ as in (5.10). We can then follow the proof of Theorem 5.1 to conclude that, for $(\tilde{q}(0), v(0)) \in \mathcal{S}\times\mathbb{R}^{2n}$, $e = 0$ is exponentially stable and (3.1) holds.

Now, since $e(t) \to 0$ as $t \to \infty$ from the above analysis, we know from (4.7) that $z(t) \to 0$ as $t \to \infty$. Since we know $R(q)$ is bounded, then $u_a(t) \to 0$ as $t \to \infty$ from (4.11). Therefore, we have that $v_f(t) \to (\mathbf{1}_n \otimes v_d)$ as $t \to \infty$ from (5.16). Since we have proven that $s(t) \to 0$ as $t \to \infty$, it follows from (5.5) that $v(t) - v_f(t) \to 0$ as $t \to \infty$. Therefore, $v_i(t) - v_d(t) \to 0$ as $t \to \infty$, $i = 1, ..., n$. ■

Remark 5.3 The control (5.8) and (5.16) can be written component-wise as follows

$$u_i = \dot{v}_d - k_v v_i - \sum_{j\in\mathcal{N}_i(E^*)} \left[\left(k_v k_q + 1\right) \tilde{q}_{ij} z_{ij} + k_q \left(z_{ij} I_2 + 2\tilde{q}_{ij}\tilde{q}_{ij}^T \right) \tilde{v}_{ij} \right]. \tag{5.17}$$

Therefore, the ith agent is only required to know the swarm acceleration in addition to the signals described in Remark 5.2.

5.1.3 Target Interception with Unknown Target Acceleration

Given the control objective (3.3), we consider that q_T is a $\mathcal{C}^2$ function and $q_T(t), \dot{q}_T(t), \ddot{q}_T(t) \in \mathcal{L}_\infty$. Here, we will assume the signals $q_T - q_n$, $\dot{q}_T - \dot{q}_n$, and $\dot{q}_T$ are known and can be broadcast to the followers; however, $\ddot{q}_T$ is *unknown*.

The theorem below gives the main result of this section.

Theorem 5.3 Let the initial conditions of (5.1) be such that $(\tilde{q}(0), v(0)) \in \mathcal{S}\times\mathbb{R}^{2n}$ where $\mathcal{S}$ was defined in Theorem 4.1. Consider the control

$$u = -k_v s + h_d - R^T(q)\, z \tag{5.18}$$

where s was defined in (5.5),

$$v_f = u_a + \mathbf{1}_n \otimes \left(v_T + k_T e_T\right), \tag{5.19}$$

$$h_d = \dot{u}_a - k_s \text{sgn}(s) + \mathbf{1}_n \otimes k_T \dot{e}_T, \tag{5.20}$$

u_a was defined in (4.11), e_T was defined in (4.19), $k_v, k_T > 0$, and $k_s \geq \sqrt{n}\left\|\dot{v}_T\right\|_{\mathcal{L}_\infty}$. Then, (5.18)

in closed loop with (5.1) renders $(e, s) = 0$ exponentially stable and ensures that (3.1) and (3.3) are satisfied.

Proof. Substituting (5.18) into (5.7) along with (4.11), (5.19), and (5.20), and then applying Lemma 2.3 gives

$$\begin{aligned} \dot{W}_d &= -k_q z^T R R^T z - k_v s^T s + s^T \left(h - \dot{v}_f\right) \\ &\leq -k_q z^T R R^T z - k_v s^T s + \|s\|_2 \left(\sqrt{n}\left\|\dot{v}_T\right\|_{\mathcal{L}_\infty} - k_s\right). \end{aligned} \tag{5.21}$$

Given that $k_s \geq \sqrt{n}\left\|\dot{v}_T\right\|_{\mathcal{L}_\infty}$, we can follow the proof of Theorem 5.1 to show that (5.11) follows from (5.21) for $(\tilde{q}(0), v(0)) \in \mathcal{S}\times\mathbb{R}^{2n}$. Therefore, we know that $(e, s) = 0$ is exponentially stable and (3.1) holds.

Now, note from (5.19) that

$$v_{fn} = u_{an} + v_T + k_T e_T \tag{5.22}$$

where the subscript n denotes the nth element of the corresponding vector. Differentiating (4.19) and applying (5.22) yields

$$\begin{aligned} \dot{e}_T &= v_T - v_n = v_T - (v_{fn} + s_n) \\ &= -k_1 e_T + r \end{aligned} \tag{5.23}$$

where $r := -s_n - u_{an}$. Observe that (5.23) is a stable linear system with input r. Since $(e, s) = 0$ is exponentially stable, we can show as in the proof of Theorem 5.2 that $u_a(t) \to 0$ as $t \to \infty$. Therefore, $r(t) \in \mathcal{L}_2$ and, from (5.23), $e_T(t) \to 0$ as $t \to \infty$ (see Theorem 2.13 in [31]).

Finally, since we know the control (5.18) ensures $q_n(t) \in \text{conv}\{q_1(t), q_2(t), ..., q_{n-1}(t)\}$ as $t \to \infty$ due to the manner in which F^* is constructed, we conclude from the convergence of (4.19) to zero that (3.3) holds. ■

Remark 5.4 The control (5.18) can be written component-wise as follows

$$\begin{aligned} u_i &= -k_v v_i + k_v\left(v_T + k_T e_T\right) + k_T \dot{e}_T \\ &\quad - \sum_{j\in\mathcal{N}_i(E^*)} \left[k_q\left(z_{ij} I_2 + 2\tilde{q}_{ij}\tilde{q}_{ij}^T\right)\tilde{v}_{ij} + \left(k_v k_q + 1\right)\tilde{q}_{ij} z_{ij}\right] \\ &\quad -k_s \text{sgn}(v_i - v_T - k_T e_T + k_q \sum_{j\in\mathcal{N}_i(E^*)} \tilde{q}_{ij} z_{ij}). \end{aligned} \tag{5.24}$$

Therefore, in addition to the signals described in Remark 5.2, the control input for each agent is a function of the target velocity and target relative position/velocity to the leader.

5.2 Simulation Results

Simulations were conducted to demonstrate the performance of the proposed control laws for the double-integrator model.

5.2.1 Formation Acquisition

The desired formation was the regular convex pentagon given in Section 4.2.1. The initial conditions of the agents were selected by

$$\begin{aligned} q_i(0) &= q_i^* + \delta_1 \left[\text{rand}(0,1) - 0.5\mathbf{1}_2\right] \quad \text{and} \\ v_i(0) &= \delta_2 \left[\text{rand}(0,1) - 0.5\mathbf{1}_2\right], \quad i = 1, \ldots, 5 \end{aligned} \tag{5.25}$$

with $\delta_1 = 1$, $\delta_2 = 0.1$. Both control gains k_q and k_v in (5.8) were set to 1. Figure 5.1 shows the trajectories of the five agents forming the desired shape (up to rotation and translation), while Figure 5.2 shows the distance errors $e_{ij}(t)$, $i, j \in V^*$ approaching zero. The x- and y-direction components of the control inputs $u_i(t)$, $i = 1, \ldots, 5$ are given in Figure 5.3.

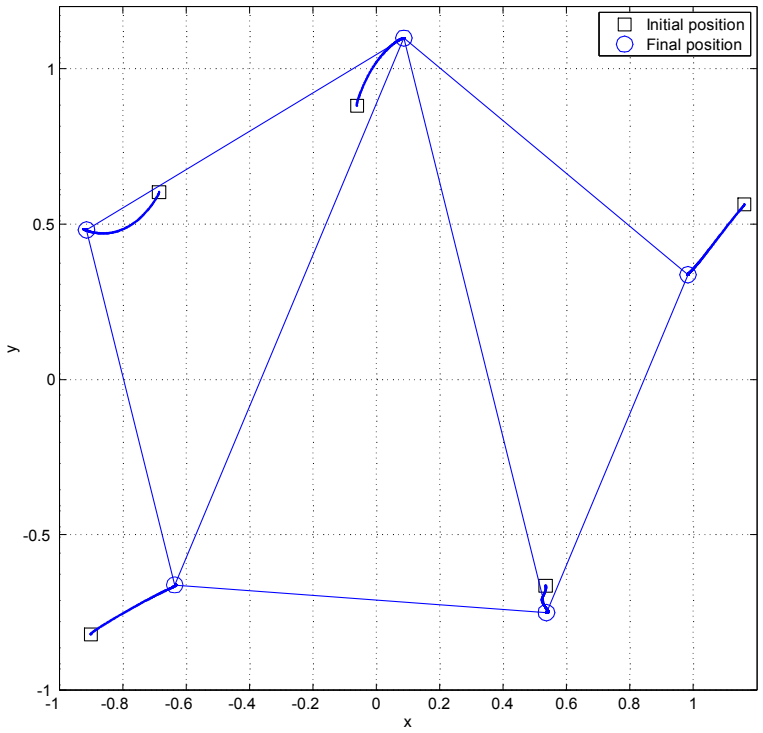

Figure 5.1: Double-integrator formation acquisition: agent trajectories $q_i(t)$, $i = 1, ..., 5$.

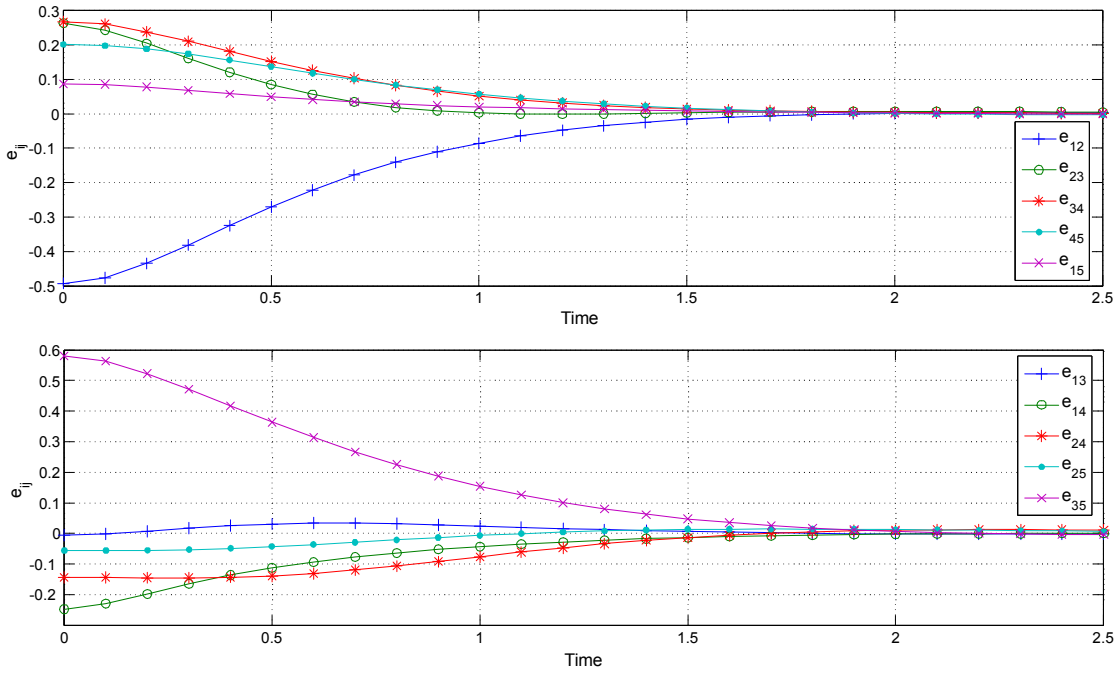

Figure 5.2: Double-integrator formation acquisition: distance errors $e_{ij}(t)$, $i, j \in V^*$.

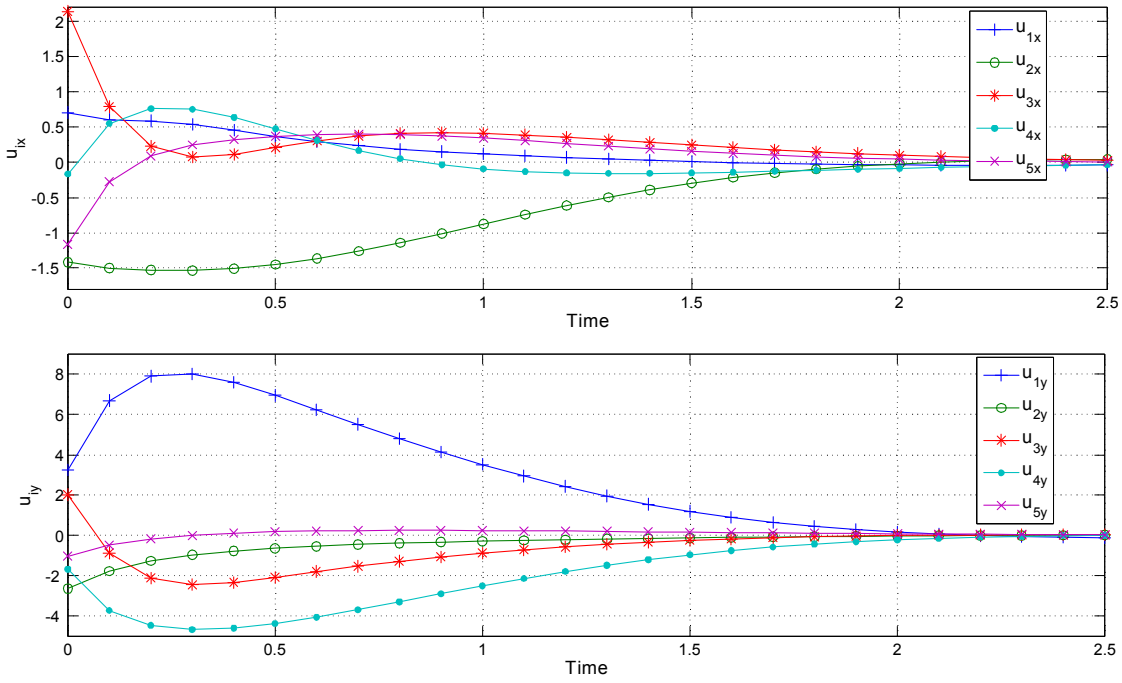

Figure 5.3: Double-integrator formation acquisition: control inputs $u_i(t)$ $i = 1, \ldots, 5$.

5.2.2 Formation Maneuvering

The desired formation was the same as above. The desired swarm velocity was set to (4.36) and the initial conditions of the agents were selected by (5.25) with $\delta_1 = 1$, $\delta_2 = 2$. The control gains k_q and k_v were set to 0.2 and 1, respectively.

Figure 5.4 shows the agent trajectories over time as they acquire and maintain the desired formation, while translating according to (4.36). The arrows in Figure 5.4 indicate the direction of each agent velocity, which eventually become tangent to the desired trajectory given from (4.36). Figure 5.5 shows the inter-agent distance errors $e_{ij}(t)$, $i, j \in V^*$ approaching zero. The x- and y-direction components of the control inputs $u_i(t)$, $i = 1, \ldots, 5$ are given in Figure 5.6. Notice that in the x (resp., y) direction, the control inputs converge to 0 (resp., $-\sin t$), the derivative of the first (resp., second) element of (4.36).

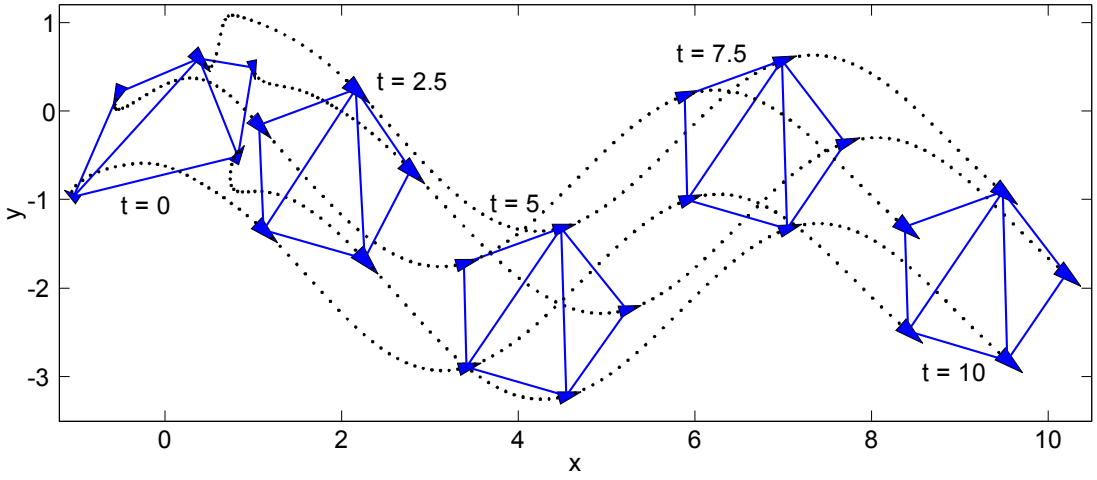

Figure 5.4: Double-integrator formation maneuvering: agent trajectories $q_i(t)$, $i = 1, ..., 5$.

5.2.3 Target Interception

The desired formation was the regular convex pentagon with the leader (agent 6) located at the origin as in Section 4.2.3. The velocity of the moving target was set to (4.37) with initial position $q_T(0) = (2, 0)$.

The initial conditions were set by (5.25) with $i = 1, ..., 6$, $\delta_1 = 1$, and $\delta_2 = 2$. The control gains in (5.18) were set to $k_q = 0.7$, $k_v = 0.1$, $k_T = 0.5$, and $k_s = 3$. The value for k_s was selected according to the inequality in Theorem 5.3 since, from (4.37), $\|\dot{v}_T\|_{\mathcal{L}_\infty} = 1$. Figure 5.7 shows the leader gradually approaching the moving target and "locking" on to it at about $t =$

5. Simultaneously, the followers successfully surround the target forming the desired pentagon. Figure 5.8 shows all the inter-agent distance errors converging to zero. Figure 5.9 shows the control inputs of each agent along the x and y directions.

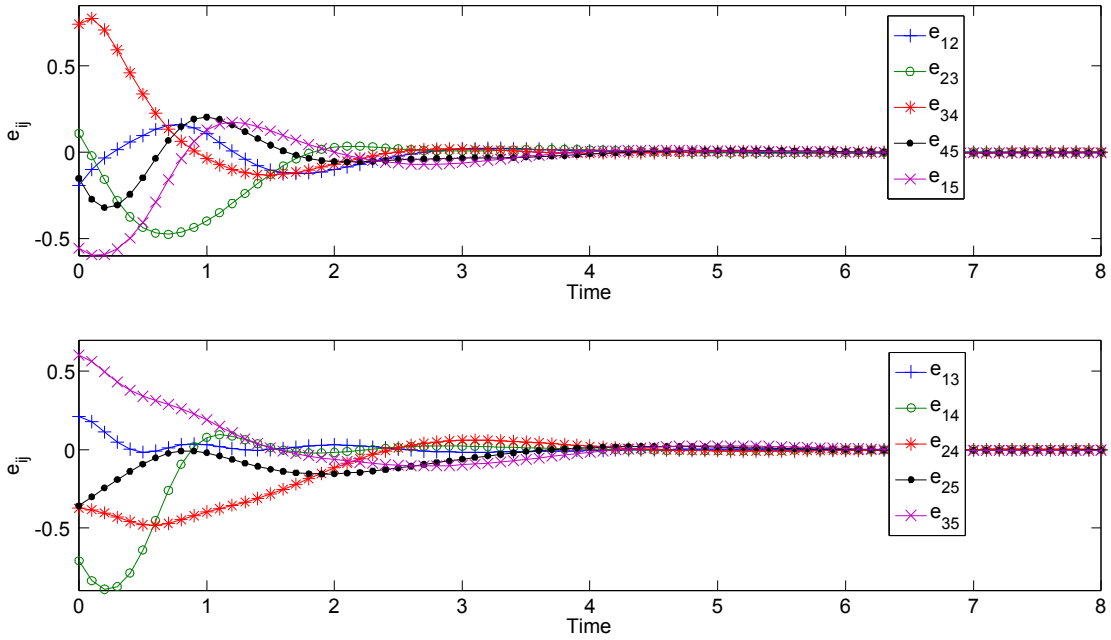

Figure 5.5: Double-integrator formation maneuvering: inter-agent distance errors for $i, j \in V^*$.

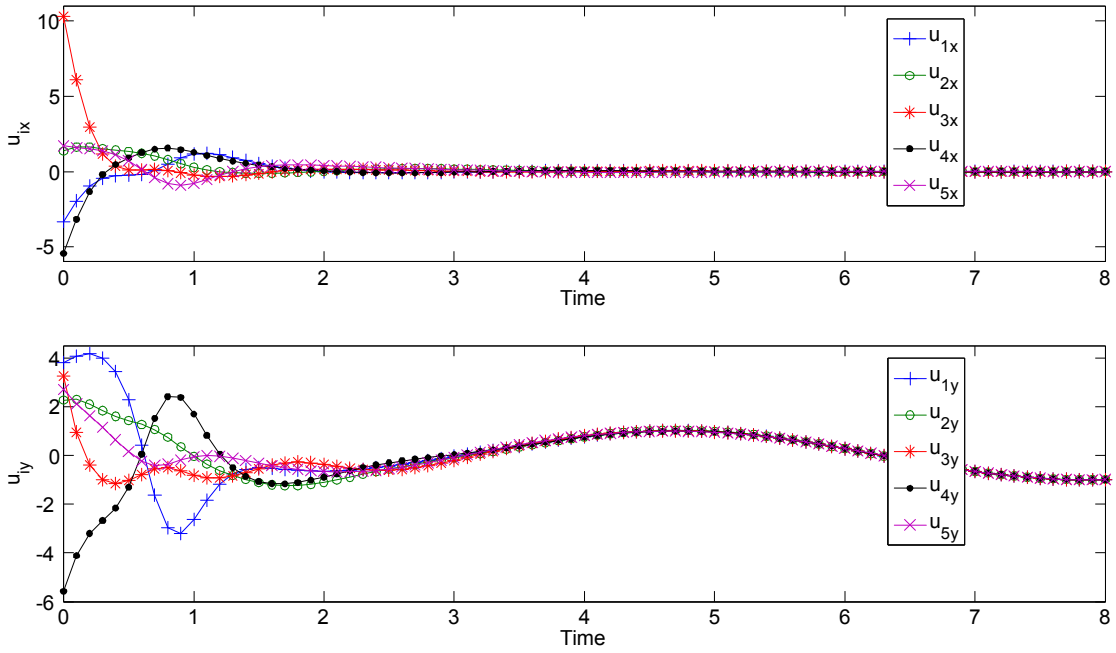

Figure 5.6: Double-integrator formation maneuvering: control inputs along x and y directions.

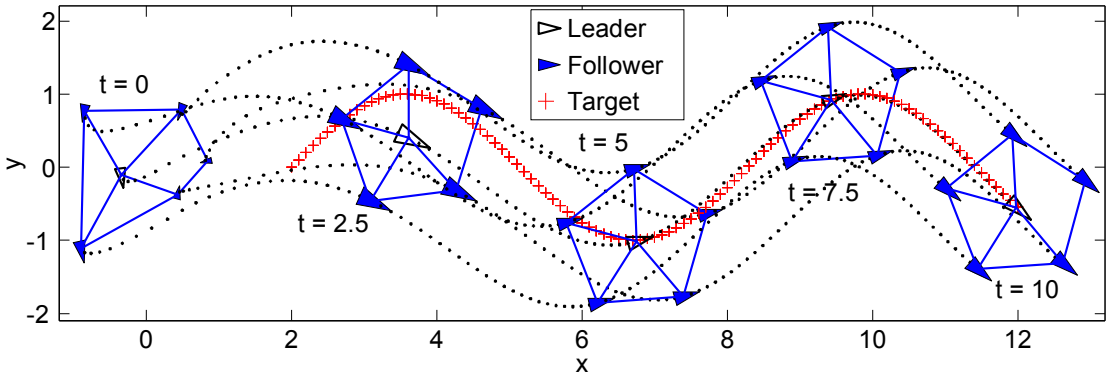

Figure 5.7: Double-integrator target interception: agent and target trajectories.

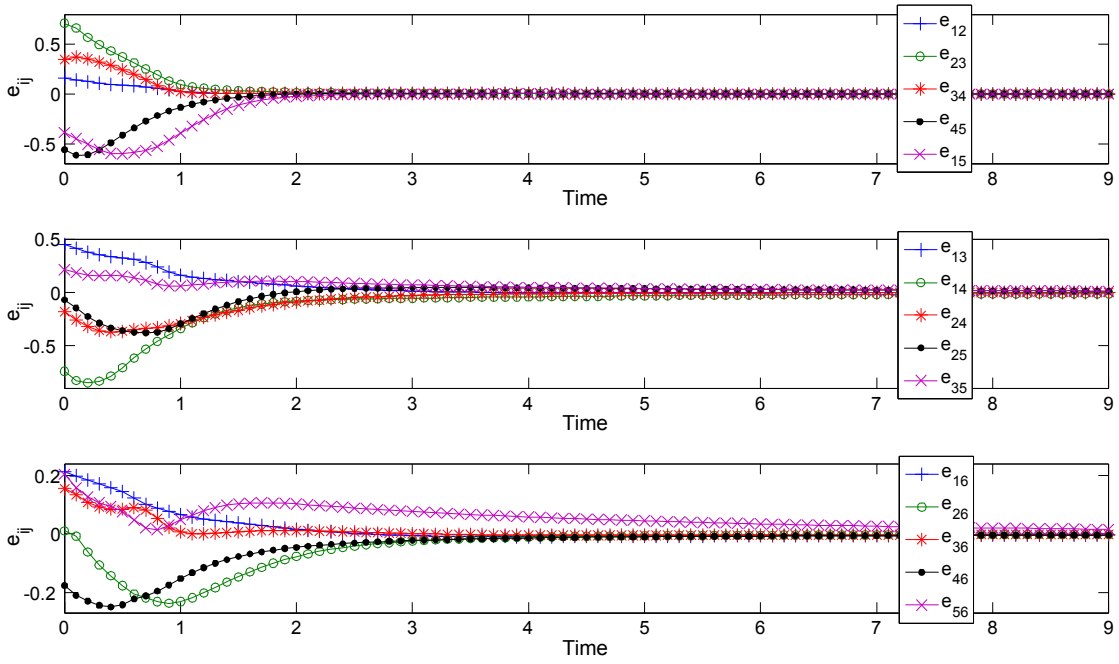

Figure 5.8: Double-integrator target interception: inter-agent distance errors for $i, j \in V^*$.

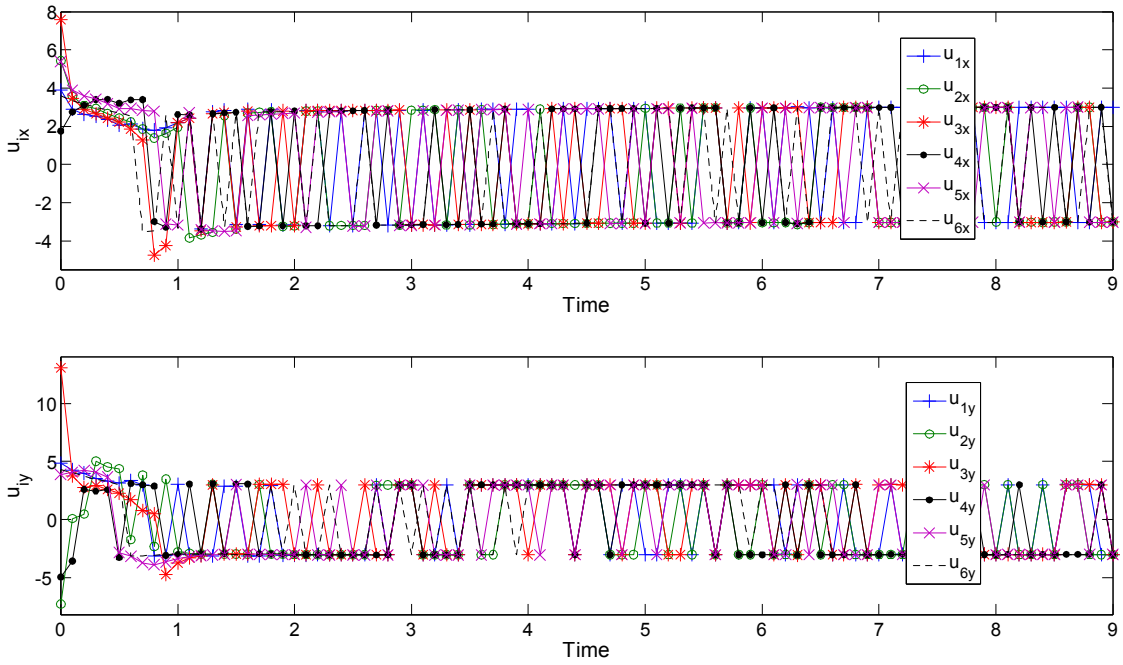

Figure 5.9: Double-integrator target interception: control inputs along x and y directions.

Chapter 6 Mechanical Dynamic Model

In this chapter, we will include in the multi-agent system model the mechanical dynamics of each agent. To this end, we consider a heterogenous system of n underactuated robotic vehicles moving autonomously in the plane. Figure 6.1 depicts the ith vehicle, where the reference frame $\{X_0, Y_0\}$ is fixed to the Earth. The moving reference frame $\{X_i, Y_i\}$ is attached to the ith vehicle with the X_i-axis aligned with its heading direction, which is given by the angle θ_i. Point C_i denotes the ith vehicle center of mass, which we assume coincides with its center of rotation. We assume the following model for the vehicles [13, 17, 29]

$$\dot{p}_{ci} = S(\theta_i)\,\eta_i \tag{6.1a}$$

$$\bar{M}_i\dot{\eta}_i + \bar{D}_i\eta_i = \bar{u}_i \tag{6.1b}$$

for $i = 1, \ldots, n$. In (6.1a), $p_{ci} = (x_{ci}, y_{ci}, \theta_i)$ is the position and orientation of $\{X_i, Y_i\}$ relative to $\{X_0, Y_0\}$, $\eta_i = (\nu_i, \dot{\theta}_i)$, ν_i is the ith robot's translational speed in the direction of θ_i, $\dot{\theta}_i$ is the ith robot's angular speed about the vertical axis passing through C_i, and

$$S(\theta_i) = \begin{bmatrix} \cos\theta_i & 0 \\ \sin\theta_i & 0 \\ 0 & 1 \end{bmatrix}. \tag{6.2}$$

In (6.1b), $\bar{M}_i = \text{diag}(m_i, J_i)$, m_i is the ith vehicle mass, J_i is the ith vehicle moment of inertia about the vertical axis, $\bar{D}_i \in \mathbb{R}^{2\times 2}$ is the constant damping matrix, and $\bar{u}_i \in \mathbb{R}^2$ represents the force/torque-level control input provided by the actuation system. The model (6.1) represents a class of underactuated robotic vehicles that includes wheeled mobile robots, marine vessels, underwater vehicles with constant depth, and aircraft with constant altitude. The system is underactuated in the sense that it has three degrees-of-freedom on the plane but only two control inputs.

To facilitate the subsequent control design, we proceed as in [25, 40] and define the following "hand" position $q_i = (x_i, y_i)$ for the ith robot relative to $\{X_0, Y_0\}$ (point H_i in Figure 6.1)

$$q_i = \begin{bmatrix} x_{ci} \\ y_{ci} \end{bmatrix} + L_i \begin{bmatrix} \cos\theta_i \\ \sin\theta_i \end{bmatrix}. \tag{6.3}$$

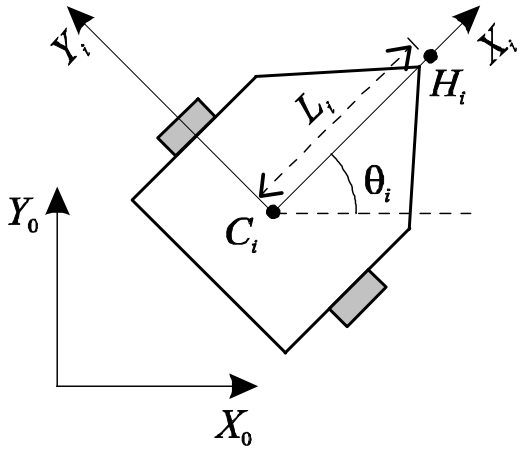

Figure 6.1: The ith robotic vehicle.

From (6.1a), (6.2), and (6.3), we have that

$$\eta_i = \Lambda(\theta_i)\,\dot{q}_i, \quad \Lambda(\theta_i) = \begin{bmatrix} \cos\theta_i & \sin\theta_i \\ -(\sin\theta_i)/L_i & (\cos\theta_i)/L_i \end{bmatrix}. \tag{6.4}$$

After taking the time derivative of (6.4) and pre-multiplying the resulting equation by $\bar{M}_i$, we obtain

$$\bar{u}_i - \bar{D}_i\Lambda(\theta_i)\,\dot{q}_i = \bar{M}_i\dot{\Lambda}(\theta_i)\,\dot{q}_i + \bar{M}_i\Lambda(\theta_i)\,\ddot{q}_i \tag{6.5}$$

where (6.1b) was used. Now, pre-multiplying (6.5) by $J^T(\theta_i)$, we arrive at

$$M_i(q_i)\,\ddot{q}_i + C_i(q_i,\dot{q}_i)\dot{q}_i + D_i(q_i)\,\dot{q}_i = u_i \tag{6.6}$$

where

$$\begin{aligned} &M_i = \Lambda^T\bar{M}_i\Lambda, \quad C_i = \Lambda^T\bar{M}_i\dot{\Lambda}, \quad D_i = \Lambda^T\bar{D}_i\Lambda, \\ &\text{and} \quad u_i = \Lambda^T\bar{u}_i. \end{aligned} \tag{6.7}$$

The expressions for the mass matrix $M_i(q_i)$ and Coriolis/centripetal matrix $C_i(q_i,\dot{q}_i)$ are given in Appendix C.

The transformed dynamics (6.6) satisfy the following properties, which can be easily verified from the expressions in Appendix C.

Property 1. The mass matrix is symmetric and positive definite, and

$$m_{i1}\|\mu\|_2^2 \le \mu^T M_i(q_i)\,\mu \le m_{i2}\|\mu\|_2^2 \quad \forall\mu\in\mathbb{R}^2 \tag{6.8}$$

where $m_{i2} > m_{i1} > 0$.

Property 2. The mass and Coriolis/centripetal matrices have the following skew-symmetric relationship

$$\mu^T \left(\frac{1}{2} \dot{M}_i (q_i) - C_i(q_i, \dot{q}_i) \right) \mu = 0 \quad \forall \mu \in \mathbb{R}^2. \tag{6.9}$$

6.1 Formation Acquisition

Here, we focus on the formation acquisition problem only. Specifically, we wish to design $u_i = u_i(q_i, q_i - q_j, \dot{q}_i, \dot{q}_i - \dot{q}_j, d_{ij})$ for (6.6), $i = 1, \ldots, n$ and $j \in \mathcal{N}_i (E^*)$, where $\mathcal{N}_i (\cdot)$ was defined in (2.1), such that the control objective (3.1) is achieved.

We begin by rewriting (6.6) as

$$\dot{q}_i = v_i \tag{6.10a}$$

$$M_i (q_i) \dot{v}_i = u_i - C_i(q_i, \dot{q}_i) v_i - D_i (q_i) v_i \tag{6.10b}$$

where $v_i \in \mathbb{R}^2$ represents the hand velocity of the ith robotic vehicle relative to Earth-fixed frame.

Motivated by (5.6) and (6.10), we introduce the function

$$W_d (e, s) = W (e) + \frac{1}{2} s^T M(q) s \tag{6.11}$$

where W was defined in (4.8) and $M(q) = \text{diag}(M_1(q_1), \ldots, M_n(q_n))$. After taking the time derivative of (6.11), we obtain

$$\begin{aligned} \dot{W}_d &= z^T R v + \frac{1}{2} s^T \dot{M}(q) s + s^T M(q) \dot{s} \\ &= z^T R (s + v_f) + \frac{1}{2} s^T \dot{M}(q) s + s^T \left[u - C(q, \dot{q}) \dot{q} - D (q) \dot{q} - M(q) \dot{v}_f \right] \\ &= z^T R v_f + s^T \left[u - C(q, \dot{q}) v_f - D (q) \dot{q} - M(q) \dot{v}_f + R^T (q) z \right] \end{aligned} \tag{6.12}$$

where (6.6) and (6.9) were used, $u = (u_1, ..., u_n) \in \mathbb{R}^{2n}$, $C(q, \dot{q}) = \text{diag}(C_1(q_1, \dot{q}_1), ..., C_n(q_n, \dot{q}_n))$, and $D (q) = \text{diag}(D_1(q_1), ..., D_n(q_n))$.

The control law for formation acquisition is given in the following theorem.

Theorem 6.1 Let the initial condition of (6.1) be such that $(\tilde{q}(0), v(0)) \in \mathcal{S} \times \mathbb{R}^{2n}$ where $\mathcal{S}$ is defined in Theorem 4.1. Then, the control

$$u = -k_v s + C(q, \dot{q}) v_f + D (q) \dot{q} + M (q) \dot{v}_f - R^T (q) z, \tag{6.13}$$

where

$$v_f = u_a, \tag{6.14}$$

u_a was defined in (4.11), and $k_v, k_q > 0$, renders $(e, s) = 0$ exponentially stable and ensures that (3.1) are satisfied.

Proof. Substituting (6.13) into (6.12) yields

$$\dot{W}_d = -k_q z^T R(q) R^T(q) z - k_v s^T s. \tag{6.15}$$

Now, following the proof of Theorem 4.1, we obtain

$$\begin{aligned} \dot{W}_d &\leq -k_q \lambda_{\min}\left(RR^T\right) z^T z - k_v s^T s \\ &\leq -\min\left\{k_q \lambda_{\min}\left(RR^T\right), k_v\right\}\left(\|z\|_2^2 + \|s\|_2^2\right) \\ &\leq -\beta W_d \end{aligned} \tag{6.16}$$

for $\tilde{q}(t) \in \mathcal{S}$ where

$$\beta = \frac{2\min\left\{k_q \lambda_{\min}\left(RR^T\right), k_v\right\}}{\max\left\{1/2, \max\limits_i \{m_{i2}\}\right\}} > 0 \tag{6.17}$$

and m_{i2} was defined in (6.8). Since (6.16) is negative definite, the level sets of W_d are invariant [24] and, if $\tilde{q}(0) \in \mathcal{S}$, $\tilde{q}(t)$ stays in $\mathcal{S}$ for all $t > 0$. Thus, $(e, s) = 0$ is exponentially stable for $(\tilde{q}(0), v(0)) \in \mathcal{S} \times \mathbb{R}^{2n}$ [24].

Finally, since $F(t)$ is infinitesimally rigid $\forall t \geq 0$ and flip ambiguities have been avoided, the exponentially stability of $(e, s) = 0$ implies that $\|q_i(t) - q_j(t)\|_2 \to d_{ij}$ as $t \to \infty$ for all $(i, j) \in E_g^*$. ■

Remark 6.1 It is straightforward to check that all signals remain bounded during closed-loop operation. The boundedness of e implies $\tilde{q}$ and z are bounded from (4.3) and (4.7). From (6.14), we then know v_f is bounded. Since s is bounded from Theorem 6.1, we know v is bounded from (5.5). From (5.12), we know $\dot{v}_f$ is bounded. Now, since e and s converge to zero *exponentially*, so does v (see (5.5) and (6.14)); therefore, q is bounded [9]. From (6.13), we conclude u is bounded. Since Λ^{-1} from (6.4) is bounded, we know from (6.7) that $\bar{u}_i$ $(i = 1, \ldots, n)$ is bounded. From (6.6) and (6.8), we know $\ddot{q}$ is bounded. Since Λ in (6.4) is bounded, we know η_i is bounded. Then, from (6.1a) and (6.2), we have that $\dot{p}_{ci}$ is bounded. From (6.1b), it is obvious that $\dot{\eta}_i$ is bounded. Since

$\dot{q}_i$ converges to zero exponentially, we know from (6.4) that η_i converges to zero exponentially and thus, θ_i is bounded. Finally, from (6.3), we know x_{ci} and y_{ci} are bounded.

Remark 6.2 The arguments of M_i, C_i, and D_i were given as q_i and $\dot{q}_i$ in (6.6) since these variables are the states of the transformed dynamics. However, notice from (6.7), (C.1), and (C.2) that these matrices are only dependent on θ_i and $\dot{\theta}_i$. With this in mind, the ith component of the control (6.13) can written as

$$\begin{aligned} u_i &= \left(D_i\left(\theta_i\right) - k_v I_2\right) v_i + \left[C_i(\theta_i, \dot{\theta}_i) - \left(k_v k_q + 1\right) I_2\right] \sum_{j \in \mathcal{N}_i(E^*)} \tilde{q}_{ij} z_{ij} \\ &\quad - k_q M_i\left(\theta_i\right) \sum_{j \in \mathcal{N}_i(E^*)} \left(z_{ij} I_2 + 2\tilde{q}_{ij}\tilde{q}_{ij}^T\right) \tilde{v}_{ij}. \end{aligned} \tag{6.18}$$

Thus, the ith vehicle control input is only a function of the ith heading angle, the ith velocity, and the relative position/velocity to its neighbors $\mathcal{N}_i\left(E^*\right)$, which can all be measured with onboard sensors. That is, the formation control does *not* require measurement of the center of mass position (x_{ci}, y_{ci}). As a result, the control implementation for each vehicle is still decentralized despite the dynamic compensation.

6.2 Simulation Results

A five-vehicle simulation was conducted using the following parameters

$$\begin{aligned} &m_i = 3.6 \text{ kg}, \quad J_i = 0.0405 \text{ kg-m}^2, \\ &\bar{D}_i = \begin{bmatrix} 0.3 \text{ kg/s} & 0 \\ 0 & 0.004 \text{ kg-m}^2/\text{s} \end{bmatrix}, \quad L_i = 0.15 \text{ m} \end{aligned} \tag{6.19}$$

for $i = 1, \ldots, 5$. The simulation consisted of applying control law (6.13) to (6.1) using the fact that $\bar{u}_i = \Lambda^{-T} u_i$ from (6.7).

The desired formation was the regular convex pentagon shown in Figure 4.1 and the initial position and orientation of the vehicles were set to

$$\begin{aligned} q_i(0) &= q_i^* + \delta_1 \left[\text{rand}(0,1) - 0.5\mathbf{1}_2\right], \\ \theta_i\left(0\right) &= \delta_2 \,\text{rand}(0,1), \; i = 1, \ldots, 5 \end{aligned} \tag{6.20}$$

where $\delta_1 = 1$, $\delta_2 = 2\pi$. The initial position of each vehicle's mass center (x_{ci}, y_{ci}) was then

obtained from (6.3) and (6.20). The initial translational and angular speed of each vehicle was selected as

$$\begin{aligned} \nu_i(0) &= \delta_3 \left[\mathrm{rand}(0,1) - 0.5\mathbf{1}_2\right], \\ \dot{\theta}_i(0) &= \delta_4 \left[\mathrm{rand}(0,1) - 0.5\mathbf{1}_2\right], \ i = 1, \ldots, 5 \end{aligned} \tag{6.21}$$

where $\delta_3 = \delta_4 = 1$. The control gains k_q and k_v were set to 0.5 and 2, respectively.

Figure 6.2 shows the trajectories of the robots' hand position $q_i(t)$, $i = 1, \ldots, 5$ forming the desired shape (up to rotation and translation), while Figure 6.3 shows the distance errors $e_{ij}(t)$, $i, j \in V^*$ approaching zero. The control inputs $\bar{u}_i(t)$, $i = 1, \ldots, 5$ are given in Figure 6.4.

Another simulation was conducted to study the robustness of the proposed control to parametric uncertainties. To this end, we assume there is a random $\pm 20\%$ mismatch between the inertia and damping parameters in (6.1) and corresponding parameters used by the control (6.13). Specifically, we used the values of m_i, I_i, and $\bar{D}_i$ given in (6.19) in the controller, while, when simulating (6.1), these parameters were set according to

$$\begin{aligned} \bar{M}_i^{\text{model}} &= \bar{M}_i \mathrm{diag}\left(0.4\,\mathrm{rand}(0,1) + 0.8, 0.4\,\mathrm{rand}(0,1) + 0.8\right), \\ \bar{D}_i^{\text{model}} &= \bar{D}_i \mathrm{diag}\left(0.4\,\mathrm{rand}(0,1) + 0.8, 0.4\,\mathrm{rand}(0,1) + 0.8\right), \end{aligned} \tag{6.22}$$

where $\mathrm{rand}(0,1)$ generates a random number uniformly distributed on the interval $(0,1)$. The simulation used the same desired formation, initial conditions, and control gains as in Figure 6.2. We conducted numerous simulations with the random parameters generated from (6.22), and in all of them the controller successfully ensured the vehicles converged to the desired formation. Representative results of this robustness study are shown in Figures 6.5, 6.6, and 6.7 for the case where (6.22) resulted in $\bar{M}_i^{\text{model}} = \mathrm{diag}(3.9, 0.0382)$ and $\bar{D}_i^{\text{model}} = \mathrm{diag}(0.2, 0.005)$. Observe that the system preformance is very similar to the case where no uncertainty was assumed. This suggests that the proposed model-based control is fairly robust to parametric uncertainties in the vehicle dynamic model.

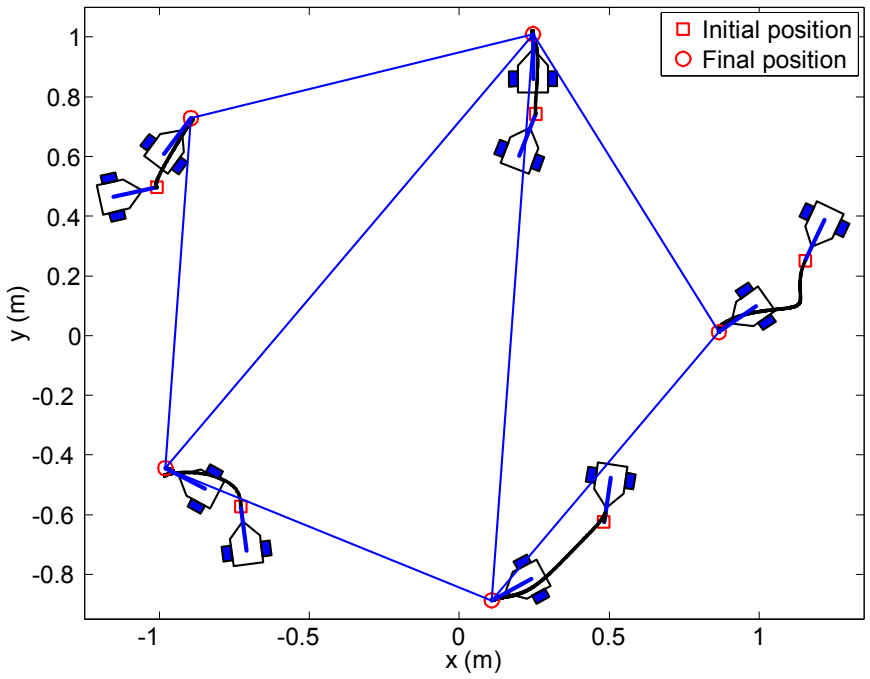

Figure 6.2: Formation acquisition with vehicle dynamics: trajectory of hand positions $q_i(t)$, $i = 1, \ldots, 5$.

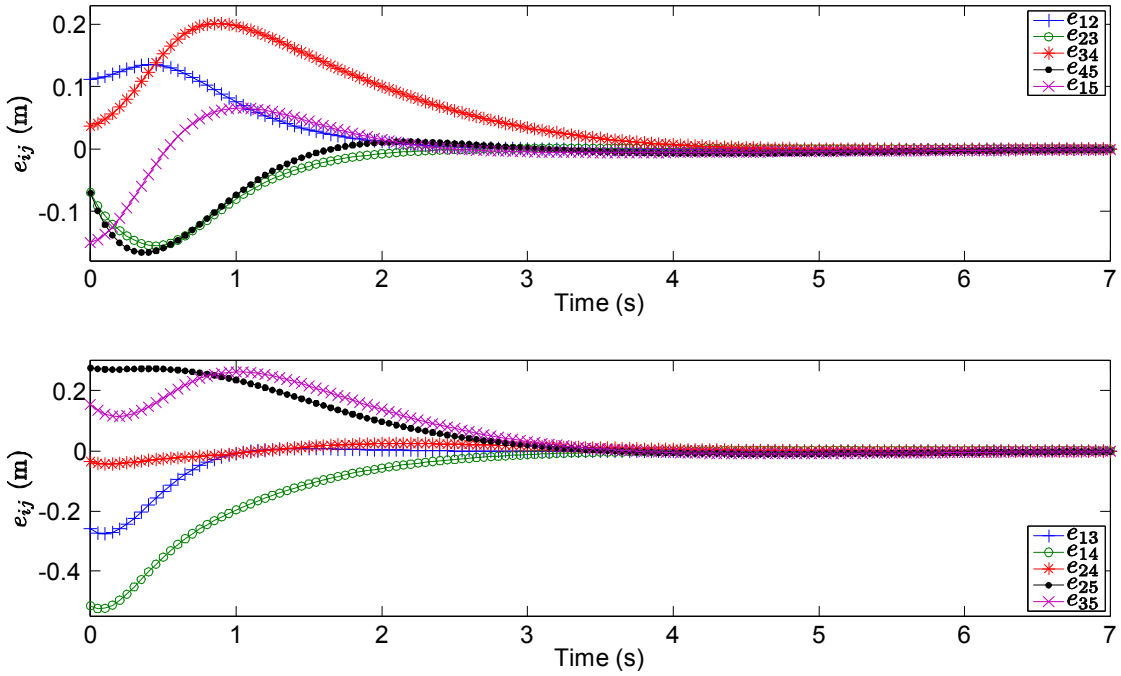

Figure 6.3: Formation acquisition with vehicle dynamics: distance errors $e_{ij}(t)$ for $i, j \in V^*$.

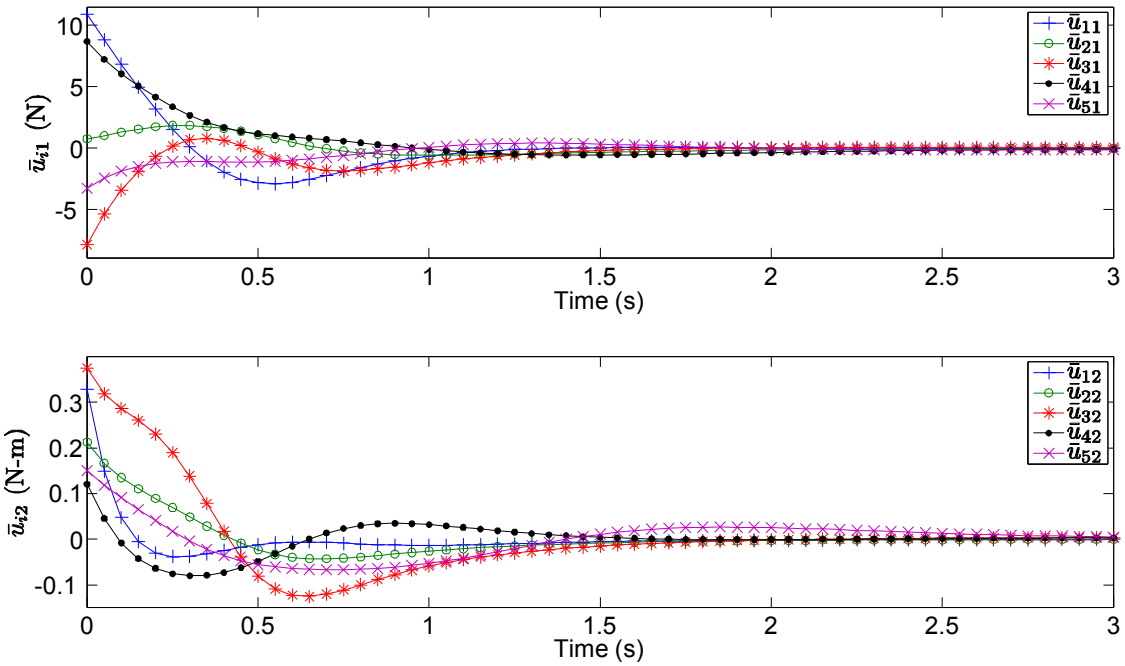

Figure 6.4: Formation acquisition with vehicle dynamics: control inputs $\bar{u}_i(t)$, $i = 1, \ldots, 5$.

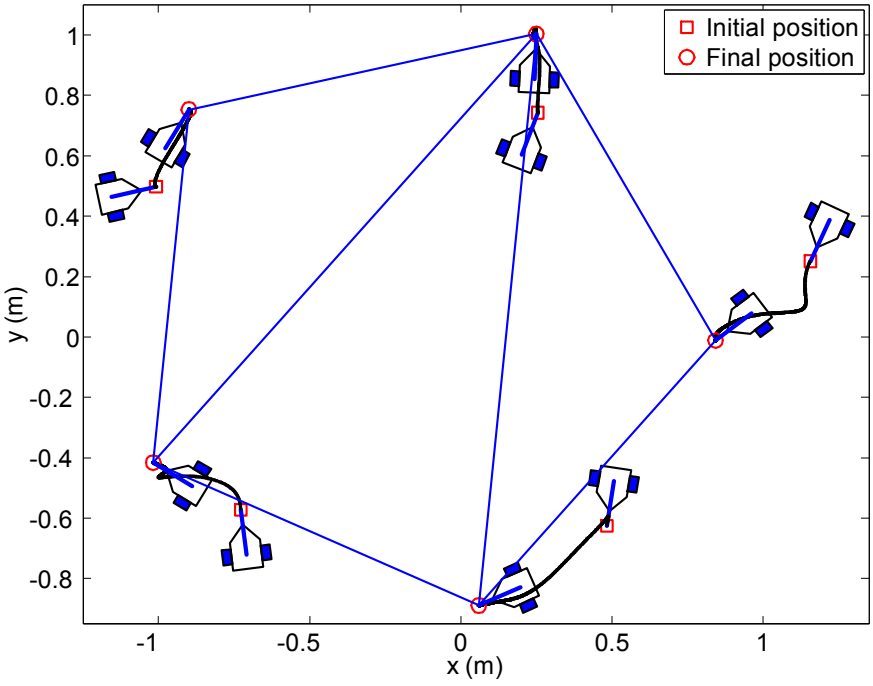

Figure 6.5: Formation acquisition with parametric uncertainties in vehicle dynamics: trajectory of hand positions $q_i(t)$, $i = 1, \ldots, 5$.

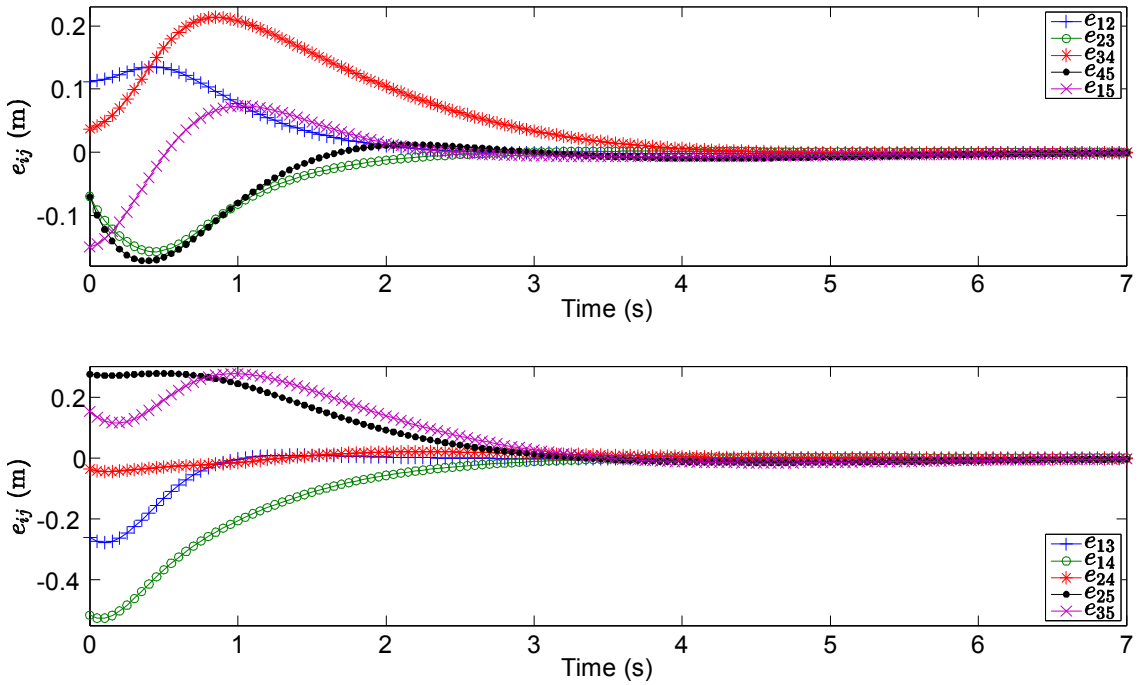

Figure 6.6: Formation acquisition with parametric uncertainties in vehicle dynamics: Distance errors $e_{ij}(t)$ for $i, j \in V^*$.

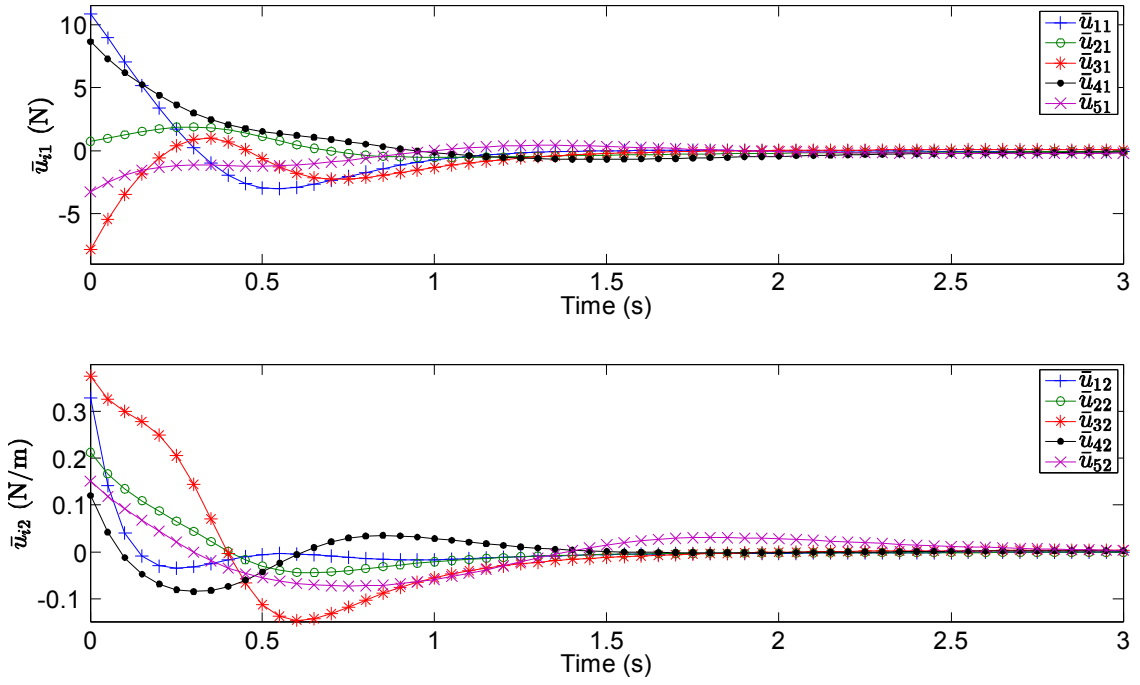

Figure 6.7: Formation acquisition with parametric uncertainties in vehicle dynamics: Control inputs $\bar{u}_i(t)$, $i = 1, \ldots, 5$.

Chapter 7 Conclusions and Future Work

This dissertation was devoted to graph rigidity-based formation control of multi-agent systems whose motion is restricted to the horizontal plane. A class of control laws was developed whose main objective was to stabilize the inter-agent distance dynamics to desired distances. Three formation problems were studied: formation acquisition, formation maneuvering, and target interception. Three types of models for the agents' motion were considered: single integrator, double integrator, and full mechanical dynamics. Rigid graph theory, Lyapunov theory, and backstepping were instrumental in solving the control problems. A summary of the three main chapters of the dissertation are as follows.

In Chapter 4, we first constructed a formation acquisition control based on the single-integrator agent model. The infinitesimal and minimal rigidity of the undirected formation graph were key properties for ensuring exponential stability to the desired formation. We then proposed formation maneuvering and target interception controls that allow the agents to converge to the desired formation while following a time-varying, swarm trajectory or tracking and surrounding a moving target with unknown velocity. A leader-follower approach was used for solving the target interception problem. The proposed controllers are composed of a formation acquisition term and a formation maneuvering or target interception term. In all three problems, we measure the relative position of agents connected in the infinitesimally and minimally rigid graph. For formation maneuvering, the desired trajectory velocity is available to all agents. In the target interception problem, the control algorithm included a term to estimate the unknown target velocity. The relative position of the target to the leader is also assumed to be measurable in the target interception case. This information is broadcast by the leader to all followers.

In Chapter 5, we showed how to construct controllers for formation acquisition, formation maneuvering, and target interception problems using the double-integrator model. Our formulation makes use of the knowledge from the previous chapter along with the backstepping method. For formation acquisition, each agent only depends on the relative position and velocity to agents to which it is connected in the infinitesimally and minimally rigid graph as well as the agent's own velocity. For formation maneuvering, the desired trajectory velocity is available to all agents. In

the target interception problem, we also measure the relative position of the target to the leader and the target absolute velocity. This information is broadcast by the leader to all followers. The target acceleration is assumed to be unknown but bounded.

In Chapter 6, a formation acquisition control law was designed for swarms of planar, underactuated, multi-robotic vehicles with dynamic effects. The backstepping control technique enabled us to rigorously embed the high-level, single-integrator-based control law from Chapter 4 into an actuator-level controller that accounts for the vehicle dynamics while ensuring exponential stability.

Several directions for future work are possible:

- Extension to agents moving in space, rather than in the plane, using concepts from 3D graph rigidity.
- Design of formation maneuvering and target interception controls with dynamic compensation.
- Consideration of uncertainties in the dynamic model.
- Development of an algorithm that selects the edges of the desired formation, for given initial conditions, to avoid the convergence of the multi-agent system to a flip formation.

References

[1] B.D.O. Anderson, C. Yu, B. Fidan, and J.M. Hendrickx, "Rigid graph control architectures for autonomous formations," *IEEE Control Syst. Mag.*, vol. 28, no. 6, pp. 48-63, 2008.

[2] L. Asimow and B. Roth, "The rigidity of graphs II," *J. Math. Anal. Appl.,* vol. 68, no. 1, pp. 171-190, 1979.

[3] J. Baillieul and A. Suri, "Information patterns and hedging Brockett's theorem in controlling vehicle formations," in *Proc. 42nd IEEE Conf. Decision and Control*, pp. 556-563, 2003.

[4] X. Cai and M. de Queiroz, "On the stabilization of planar multi-agent formations," in *Proc. ASME Conf. Dynamic Systems and Control*, Paper No. DSCC2012-MOVIC2012-8534, Ft. Lauderdale, FL, 2012.

[5] M. Cao, A.S. Morse, C. Yu, B.D.O Anderson, and S. Dasgupta, "Maintaining a directed, triangular formation of mobile autonomous agents," *Commun. Inf. Syst.*, vol. 11, no. 1, pp. 1-16, 2011.

[6] G. Chen and F.L. Lewis, "Distributed adaptive tracking control for synchronization of unknown networked Lagrangian systems," *IEEE Trans. Syst., Man, Cybern. - Part B*, Vol. 41, No. 3, pp. 805-816, 2011.

[7] S.-J. Chung and J.-J. Slotine, "Cooperative robot control and concurrent synchronization of Lagrangian systems," *IEEE Trans. Rob.*, Vol. 25, No. 3, pp. 686-700, 2009.

[8] R. Connelly, "Generic global rigidity," *Discrete Comput. Geom.*, vol. 33, no. 4, pp. 549-563, 2005.

[9] D. M. Dawson, J. Hu, and T. C. Burg, *Nonlinear control of electric machinery*, New York, NY: Marcel Dekker, 1998.

[10] J.P. Desai, J. Ostrowski, and V. Kumar, "Controlling formations of multiple mobile robots," in *Proc. IEEE Intl. Conf. Robotics & Automation*, pp. 2864-2869, 1998.

[11] R. Diestel, *Graph theory*. New York: Springer-Verlag, 1997.

[12] D.V. Dimarogonas and K.J. Kyriakopoulos, "Connectedness preserving distributed swarm aggregation for multiple kinematic robots," *IEEE Trans. Robot.*, vol. 24, no. 5, pp. 1213-1223, 2008.

[13] W.E. Dixon, D.M. Dawson, E. Zergeroglu, and A. Behal, *Nonlinear control of wheeled mobile robots*, London: Springer, 2001.

[14] F. Dörfler and B. Francis, "Formation control of autonomous robots based on cooperative behavior," in *Proc. European Control Conf.*, pp. 2432-2437, 2009.

[15] F. Dörfler and B. Francis, "Geometric analysis of the formation problem for autonomous robots," *IEEE Trans. Autom. Control*, vol 55, no. 10, pp. 2379-2384, 2010.

[16] T. Eren, P. N. Belhumeur, and A. S. Morse, "Closing ranks in vehicle formations based on rigidity," in *Proc. IEEE Conf. on Decision and Control*, pp. 2959-2964, 2002.

[17] Y. Fang, E. Zergeroglu, M.S. de Queiroz, and D.M. Dawson, "Global output feedback control of dynamically positioned surface vessels: an adaptive control approach," *Mechatronics*, Vol. 14, No. 4, pp. 341-356, 2004.

[18] J.A. Fax and R.M. Murray, "Information flow and cooperative control of vehicle formations," *IEEE Trans. Autom. Control*, vol 49, no. 9, pp. 1465-1476, 2004.

[19] J.N. Franklin, *Matrix theory*. Englewood Cliffs, New Jersey: Prentice Hall, 1968.

[20] V. Gazi and K.M. Passino, *Swarm stability and optimization*, Berlin: Springer, 2011.

[21] Y. Hong, L. Gao, D. Cheng, and J. Hu, "Lyapunov-based approach to multiagent systems with switching jointly conencted interconnections," *IEEE Trans. Autom. Control*, Vol. 52, No. 5, pp. 943-948, 2007.

[22] I. Izmestiev, "Infinitesimal Rigidity of Frameworks and Surfaces," *Lectures on Infinitesimal Rigidity*, Kyushu University, Japan, 2009.

[23] B. Jackson, "Notes on the rigidity of graphs," *Notes of the Levico Conference*, 2007.

[24] H.K. Khalil, *Nonlinear systems,* 3rd ed.. Englewood Cliffs, New Jersey: Prentice Hall, 2002.

[25] S. Khoo, L. Xie, and Z. Man, "Robust finite-time consensus tracking algorithm for multirobot systems," *IEEE/ASME Trans. Mechatronics*, Vol. 14. No. 2, pp. 219-228, 2009.

[26] L. Krick, M.E. Broucke, and B.A. Francis, "Stabilization of infinitesimally rigid formations of multi-robot networks," *Intl. J. Control*, vol 83, no. 3, pp. 423-439, 2009.

[27] M. Krstic, I. Kanellakopoulos, and P. Kokotovic, *Nonlinear and adaptive control design*. New York, NY: John Wiley & Sons, 1995.

[28] D. Lee and P.Y. Li, "Passive decomposition appraoch to formation and maneuver control of multiple rigid-bodies," *ASME J. Dyn. Syst., Measur., and Control*, Vol. 129, No. 5, pp. 662-677, 2007.

[29] Y. Liang and H.-H Lee, "Decentralized formation control and obstacle avoidance for multiple robots with nonholonomic constraints," *Proc. American Control Conf.*, pp. 5596-5601, Minneapolis, MN, 2006.

[30] D. Meng, Y. Jia, J. Du, and F. Yu, "Tracking control over a finite interval for multi-agent systems with a time-varying reference trajectory," *Systerms Control Lett.*, vol. 61, no. 7, pp. 807-818, 2012.

[31] K.S. Narendra and A.M. Annaswamy, *Stable Adaptive Systems*. Mineola, NY: Dover, 2005.

[32] P. Ögren, E. Fiorelli, and N.E. Leonard, "Cooperative control of mobile sensor networks: adaptive gradient climbing in a distributed environment," *IEEE Trans. Autom. Control*, Vol. 49, No. 8, pp. 1292-1302, 2004.

[33] K.-K. Oh, and H.-S. Ahn, "Formation control of mobile agents based on inter-agent distance dynamics," *Automatica*, vol. 47, no. 10, pp. 2306-2312, 2011.

[34] K.-K. Oh, and H.-S. Ahn, "Distance-based control of cycle-free persistent formations," in *Proc. IEEE Multi-Conf. Systems and Control*, pp. 816-821, 2011.

[35] R. Olfati-Saber and R.M. Murray, "Distributed cooperative control of multiple vehicle formations using structural potential functions," Presented at the *15th IFAC World Congress*, Barcelona, Spain, 2002.

[36] R. Olfati-Saber, Flocking for multi-agent dynamic systems: algorithms and theory. *IEEE Trans. Autom. Control*, vol. 51, no. 3, pp. 401-420, 2006.

[37] R. Olfati-Saber and P. Jalalkamali, "Coupled distributed estimation and control for mobile sensor networks," *IEEE Trans. Autom. Control*, DOI: 10.1109/TAC.2012.2190184.

[38] Z. Peng, D. Wang, Z. Chen, X. Hu, and W. Lan, "Adaptive dynamic surface control for formations of autonomous surface vehicles with uncertain dynamics," *IEEE Trans. Control Syst. Tech.*, Vol. 21, No. 2, pp. 513-520, 2013.

[39] A.R. Pereira, L. Hsu, and R. Ortega, "Globally stable adaptive formation control of Euler-Lagrange agents via potential functions," *Proc. American Control Conf.*, pp. 2606-2611, St. Louis, MO, 2009.

[40] J.-B. Pomet, B. Thuilot, G. Bastin, and G. Campion, "A hybrid strategy for the feedback stabilization of nonholonomic mobile robots," *Proc. IEEE Intl. Conf. Rob. Autom.*, pp. 129-134, Nice, France, 1992.

[41] W. Ren and R.W. Beard, *Distributed consensus in multi-vehicle cooperative control*, London: Springer-Verlag, 2008.

[42] B. Roth, "Rigid and Flexible Frameworks," *The Amer. Math. Monthly,* vol. 86, no. 1, pp. 6-21, 1981.

[43] D.J. Stilwell, B.E. Bishop, and C.A. Sylvester, "Redundant manipulator techniques for partially decentralized path planning and control of a platoon of autonmous vehicles," *IEEE Trans. Syst., Man, and Cybern. - Part B*, Vol. 35, No. 4, pp. 842-848, 2005.

[44] T.H. Summers, C. Yu, S. Dasgupta, and B.D.O Anderson, "Control of minimally persistent leader-remote-follower and coleader formations in the plane," *IEEE Trans. Autom. Control*, vol. 56, no. 12, pp. 2778-2792, 2011.

[45] P. Tabuada, G.J. Pappas, and P. Lima, "Feasible formations of multi-agent systems," in *Proc. American Control Conf.*, pp. 56-61, 2001.

[46] B. Xian, D.M. Dawson, M. de Queiroz, and J. Chen, "A continuous ssymptotic tracking control strategy for uncertain nonlinear systems," *IEEE Trans. Autom. Control*, vol. 48, no. 7, pp. 1206-1211, 2004.

[47] F. Xiao, L. Wang, J. Chen, and Y. Gao, "Finite-time formation control for multi-agent systems," *Automatica*, vol. 45, no. 11, pp. 2605-2611, 2009.

Appendix A: Proof of Lemma 4.1

Given that $\text{dist}(\bar{p}, \mathcal{H}(p)) \leq \varepsilon$, we know from Lemma 2.1 that

$$q_i = \bar{T}\left(q_i^*\right) + \delta_i\left(\varepsilon\right),\ i = 1, ..., n \tag{A.1}$$

for $\bar{T} \in \text{Iso}(\mathbb{R}^2)$. It is easy to see that d_{ij} can be written as

$$d_{ij} = \sqrt{\left[\bar{T}\left(q_i^*\right) - \bar{T}\left(q_j^*\right)\right]^T \left[\bar{T}\left(q_i^*\right) - \bar{T}\left(q_j^*\right)\right]},\ (i,j) \in E^*. \tag{A.2}$$

Therefore, from (4.2), (4.5), (4.6), (A.1), and (A.2), the Lyapunov function candidate (4.8) can be upper bounded as follows

$$\begin{aligned}
W(e) &= \frac{1}{4}\sum_{(i,j)\in E^*}\left(\|\tilde{q}_{ij}\|_2^2 - d_{ij}^2\right)^2 \\
&= \frac{1}{4}\sum_{(i,j)\in E^*}\left[\left(q_i - q_j\right)^T\left(q_i - q_j\right) - \left(\bar{T}\left(q_i^*\right) - \bar{T}\left(q_j^*\right)\right)^T\left(\bar{T}\left(q_i^*\right) - \bar{T}\left(q_j^*\right)\right)\right]^2 \\
&= \frac{1}{4}\sum_{(i,j)\in E^*}\Big[\left(\bar{T}\left(q_i^*\right) - \bar{T}\left(q_j^*\right) + \delta_i - \delta_j\right)^T\left(\bar{T}\left(q_i^*\right) - \bar{T}\left(q_j^*\right) + \delta_i - \delta_j\right) \\
&\quad - \left(\bar{T}\left(q_i^*\right) - \bar{T}\left(q_j^*\right)\right)^T\left(\bar{T}\left(q_i^*\right) - \bar{T}\left(q_j^*\right)\right)\Big]^2 \\
&= \frac{1}{4}\sum_{(i,j)\in E^*}\left[2\left(\bar{T}\left(q_i^*\right) - \bar{T}\left(q_j^*\right)\right)^T\left(\delta_i - \delta_j\right) + \left(\delta_i - \delta_j\right)^T\left(\delta_i - \delta_j\right)\right]^2 \\
&\leq \frac{1}{4}\sum_{(i,j)\in E^*}\left[2\left\|\bar{T}\left(q_i^*\right) - \bar{T}\left(q_j^*\right)\right\|_2\left\|\delta_i - \delta_j\right\|_2 + \left\|\delta_i - \delta_j\right\|_2^2\right]^2 \\
&= \frac{1}{4}\sum_{(i,j)\in E^*}\left[\left(2d_{ij} + \left\|\delta_i - \delta_j\right\|_2\right)^2\left\|\delta_i - \delta_j\right\|_2^2\right] \\
&\leq \frac{1}{4}\sum_{(i,j)\in E^*}\left[\left(2d_{ij} + \left\|\delta_i\right\|_2 + \left\|\delta_j\right\|_2\right)^2\left(\left\|\delta_i\right\|_2 + \left\|\delta_j\right\|_2\right)^2\right] =: c.
\end{aligned} \tag{A.3}$$

The boundedness of the level surfaces in (A.3) stems from the fact that (4.8) is radially unbounded.

Appendix B: Proof of Lemma 4.2

Integrating (4.21) over time gives

$$\begin{aligned}\int_0^t L(\tau)\,d\tau &= \int_0^t \left(k_1 e_T(\tau)+\dot{e}_T(\tau)\right)^T\left[\dot{v}_T(\tau)-k_2\text{sgn}\left(e_T(\tau)\right)\right]d\tau \\ &= \int_0^t k_1 e_T^T(\tau)\left[\dot{v}_T(\tau)-k_2\text{sgn}\left(e_T(\tau)\right)\right]d\tau+\int_0^t \dot{e}_T^T(\tau)\,\dot{v}_T(\tau)\,d\tau \\ &\quad -\int_0^t k_2\dot{e}_T^T(\tau)\,\text{sgn}\left(e_T(\tau)\right)d\tau. \end{aligned} \tag{B.1}$$

After integrating by parts the second integral on the right-hand side of (B.1), we obtain

$$\begin{aligned}\int_0^t L(\tau)\,d\tau &= \int_0^t k_1 e_T^T(\tau)\left[\dot{v}_T(\tau)-k_2\text{sgn}\left(e_T(\tau)\right)\right]d\tau \\ &\quad +e_T^T(\tau)\,\dot{v}_T(\tau)\big|_0^t-\int_0^t e_T^T(\tau)\,\ddot{v}_T(\tau)\,d\tau \\ &\quad -k_2\left\|e_T(\tau)\right\|_1\big|_0^t \\ &= \int_0^t k_1 e_T^T(\tau)\left[\dot{v}_T(\tau)-\frac{1}{k_1}\ddot{v}_T(\tau)-k_2\text{sgn}\left(e_T(\tau)\right)\right]d\tau \\ &\quad +e_T^T(t)\,\dot{v}_T(t)-e_T^T(0)\,\dot{v}_T(0)-k_2\left\|e_T(t)\right\|_1+k_2\left\|e_T(0)\right\|_1. \end{aligned} \tag{B.2}$$

Using the fact that $\|x\|_1 \geq \|x\|_2$ for any $x \in \mathbb{R}^n$, we upper bound the right-hand side of (B.2) as follows

$$\begin{aligned}\int_0^t L(\tau)\,d\tau &\leq \int_0^t k_1\left\|e_T(\tau)\right\|_2\left(\left\|\dot{v}_T(\tau)\right\|_2+\frac{1}{k_1}\left\|\ddot{v}_T(\tau)\right\|_2-k_2\right)d\tau \\ &\quad +\left\|e_T(t)\right\|_2\left(\left\|\dot{v}_T(t)\right\|_2-k_2\right)+k_2\left\|e_T(0)\right\|_1-e_T^T(0)\,\dot{v}_T(0). \end{aligned} \tag{B.3}$$

Now, it is easy to see that (4.23) follows from (4.22) and (B.3). Finally, the positiveness of (4.24) follows from the fact that

$$k_2\left\|e_T(0)\right\|_1-e_T^T(0)\,\dot{v}_T(0) \geqslant \left\|e_T(0)\right\|_2\left(k_2-\left\|\dot{v}_T(0)\right\|_2\right)>0$$

if k_2 is selected according to (4.22).

Appendix C: Expressions for Matrices $M_i\left(q_i\right)$ and $C_i\left(q_i, \dot{q}_i\right)$

The matrices $M_i\left(q_i\right)$ and $C_i(q_i, \dot{q}_i)$ in (6.7) are defined as follows

$$M_i = \begin{bmatrix} m_i \cos^2\theta_i + \frac{I}{L_i^2}\sin^2\theta_i & \left(m_i - \frac{I}{L_i^2}\right)\cos\theta_i \sin\theta_i \\ \left(m_i - \frac{I}{L_i^2}\right)\cos\theta_i \sin\theta_i & m_i \sin^2\theta_i + \frac{I}{L_i^2}\cos^2\theta_i \end{bmatrix} \tag{C.1}$$

and

$$C_i = \begin{bmatrix} -\left(m_i - \frac{I}{L_i^2}\right)\dot{\theta}_i \cos\theta_i \sin\theta_i & m_i\dot{\theta}_i \cos^2\theta_i + \frac{I}{L_i^2}\dot{\theta}_i \sin^2\theta_i \\ -m_i\dot{\theta}_i \sin^2\theta_i - \frac{I}{L_i^2}\dot{\theta}_i \cos^2\theta_i & \left(m_i - \frac{I}{L_i^2}\right)\dot{\theta}_i \cos\theta_i \sin\theta_i \end{bmatrix}. \tag{C.2}$$

Vita

Xiaoyu Cai was born in Huzhou, Zhejiang Province, China. He received his bachelor's degree in mechanical engineering at Shanghai Jiao Tong Unversity in 2009. In the same year, he entered the graduate school as a direct Ph.D. student in the Department of Mechanical Engineering at Louisiana State University. He will recieve the Ph.D. degree from LSU in August 2013.